Title
Seasonal and latitudinal variability of troposphere $\Delta^{14}CO_2$: Post bomb contributions from fossil fuels, oceans, the stratosphere, and the terrestrial biosphere

Journal
Global Biogeochemical Cycles, 16(4)

ISSN
08866236

Authors
Randerson, J. T
Enting, I. G
Schuur, E. A. G
et al.

Publication Date
2002-12-01

DOI
10.1029/2002GB001876

Seasonal and latitudinal variability of troposphere $\Delta^{14}CO_2$: Post bomb contributions from fossil fuels, oceans, the stratosphere, and the terrestrial biosphere

J. T. Randerson,[1] I. G. Enting,[2] E. A. G. Schuur,[3] K. Caldeira,[4] and I. Y. Fung[5]

Received 29 January 2002; revised 27 June 2002; accepted 3 September 2002; published 5 December 2002.

[1] During the mid-1960s, large seasonal amplitudes were observed in surface measurements of $\Delta^{14}C$ in the Northern Hemisphere. These seasonal oscillations were initially caused by stratosphere-troposphere exchange, with the injection of bomb ^{14}C into the troposphere during winter and spring mixing. Here we show how fossil, ocean, and terrestrial biosphere fluxes modified the stratospheric signal during the 1960s, and the evolution of each of these components in the post bomb era. In our analysis, we used the Goddard Institute for Space Studies (GISS) atmospheric tracer model, gross ocean CO_2 fluxes from the Lawrence Livermore National Laboratory (LLNL) ocean model, and terrestrial CO_2 fluxes from a biosphere-atmosphere model driven by normalized difference vegetation index and surface air temperatures. We found that ^{14}C-depeleted respiration from the terrestrial biosphere partially canceled the ^{14}C-enriched stratosphere flux in the Northern Hemisphere in the mid and late 1960s. In more recent decades, our analysis suggested that the terrestrial biosphere contribution to the $\Delta^{14}C$ seasonal cycle reversed phase, with the terrestrial biosphere currently releasing relatively ^{14}C-enriched CO_2 that mixes with relatively depleted troposphere CO_2. The timing of this reversal depended on the residence times of carbon within the footprint of the observation station. Measurements of $\Delta^{14}C$ in respiration from tundra and boreal ecosystems in Alaska provide evidence that some boreal forests have undergone this transition, while some tundra ecosystems have not. We predict that over the next century, several features of the latitudinal profile of $\Delta^{14}C$ will substantially change because of continued fossil fuel emissions in the Northern Hemisphere, and the partial release of bomb ^{14}C that has accumulated in Southern Hemisphere oceans. *INDEX TERMS:* 0368 Atmospheric Composition and Structure: Troposphere—constituent transport and chemistry; 1610 Global Change: Atmosphere (0315, 0325); 1615 Global Change: Biogeochemical processes (4805); 3339 Meteorology and Atmospheric Dynamics: Ocean/atmosphere interactions (0312, 4504); *KEYWORDS:* radiocarbon, Suess Effect, carbon cycle, Arctic and boreal ecosystems, Amazon tree rings, meridional gradient of ^{14}C

Citation: Randerson, J. T., I. G. Enting, E. A. G. Schuur, K. Caldeira, and I. Y. Fung, Seasonal and latitudinal variability of troposphere $\Delta^{14}CO_2$: Post bomb contributions from fossil fuels, oceans, the stratosphere, and the terrestrial biosphere, *Global Biogeochem. Cycles*, *16*(4), 1112, doi:10.1029/2002GB001876, 2002.

1. Introduction

[2] At the time of the Test Ban Treaty of 1963, $^{14}CO_2$ was distributed unevenly through the atmosphere [*Telegadas*, 1971]. Nuclear fireballs had carried most bomb-produced ^{14}C into the lower stratosphere, where it was quickly oxidized to ^{14}CO and $^{14}CO_2$ [*Johnston et al.*, 1976; *Glasstone and Dolan*, 1977]. As many of the tests were conducted in the Northern Hemisphere (Table 1) [*Enting*, 1982], a significant amount of this $^{14}CO_2$ subsequently reentered the Northern Hemisphere troposphere during winter and spring when mixing occurred between the stratosphere and troposphere [*Rasch et al.*, 1994; *Holton et al.*, 1995]. Southern Hemisphere troposphere $^{14}CO_2$ concentrations lagged behind Northern Hemisphere values for several years in the mid-1960s, reflecting relatively slow inter-hemispheric mixing times and dilution from gross CO_2 exchange with oceans and the terrestrial biosphere [*Levin et al.*, 1980; *Tans*, 1981; *Nydal and Lövseth*, 1983].

[1]Divisions of Geological and Planetary Sciences and Engineering and Applied Science, California Institute of Technology, Pasadena, California, USA.
[2]CSIRO Atmospheric Research, Aspendale, Victoria, Australia.
[3]Department of Botany, University of Florida, Gainesville, Florida, USA.
[4]Climate System Modeling Group, Lawrence Livermore National Laboratory, University of California, Livermore, California, USA.
[5]Center for Atmospheric Sciences, University of California Berkeley, Berkeley, California, USA.

0886-6236/02/2002GB001876

Table 1. Hemisphere Distribution of Nuclear Weapon Tests[a]

Location	Cumulative Detonations, Mt TNT, during:		
	1945–1960	1961–1962	1964–1975
Northern Hemisphere	92.6	339.9	15.5
Southern Hemisphere	4.7	0.0	10.5
Total	97.3	339.9	26.0

[a] From [*Enting*, 1982].

[3] The injection of bomb ^{14}C into the atmosphere created large anomalies in the ratio of $^{14}CO_2$ to $^{12}CO_2$ (represented by $\Delta^{14}C$, which includes a normalization for mass dependent fractionation [*Stuiver and Polach*, 1977]). Tracing the movement of this bomb $\Delta^{14}C$ signal through the atmosphere, oceans, and terrestrial biosphere has provided significant insight about CO_2 exchange rates, transport, and carbon residence times. The vertical distribution and total inventory of bomb $\Delta^{14}C$ in the oceans constrain estimates of air-sea gas exchange and the magnitude of the ocean carbon sink [*Oeschger et al.*, 1975; *Siegenthaler*, 1983; *Hesshaimer et al.*, 1994; *Broecker et al.*, 1995; *Orr et al.*, 2001]. In the atmosphere, the dispersion of bomb ^{14}C has served as a unique test of model transport, and in particular of rates of vertical mixing in the mid and lower stratosphere of the Northern Hemisphere [*Johnston et al.*, 1976; *Mahlman and Moxim*, 1978; *Shia et al.*, 1989; *Rasch et al.*, 1994]. Within the terrestrial biosphere, $\Delta^{14}C$ measurements of respiration and organic matter serve as a major constraint on allocation and rates of litter, root, and soil carbon turnover [*Balesdent*, 1987; *Harrison et al.*, 1993; *Trumbore et al.*, 1996; *Gaudinski et al.*, 2000]. This information is essential for estimating the size of the net land carbon sink and its response to changes in disturbance or climate [*Thompson et al.*, 1996; *McGuire et al.*, 2001].

[4] While the value of atmospheric $\Delta^{14}C$ as a tracer of the carbon cycle has come largely from its mean annual secular trend, seasonal and regional variability in atmospheric $\Delta^{14}C$ is clearly visible in many contemporary observations and has the potential to provide additional information about the source, age, and magnitude of regional fluxes. In general, four processes interact with atmospheric mixing and are responsible for temporal and spatial variability of tropospheric $\Delta^{14}C$: fossil fuel emissions, ocean-atmosphere exchange, stratosphere-troposphere mixing, and terrestrial ecosystem fluxes [*Nydal and Lövseth*, 1983; *Enting and Mansbridge*, 1987]. Over the last few decades, the relative contribution of each of these processes has undergone substantial modification, as much of the bomb ^{14}C has moved from the stratosphere into the deep ocean and fossil fuel use has continued to increase.

[5] In the mid 1960s, the seasonal amplitude of $\Delta^{14}C$ exceeded 150‰ across a wide range of northern stations, including Spitsbergen, Norway (78°N), Fruholmen, Norway (71°N), Point Barrow, Alaska (68°N), Trondheim, Norway (63°N), and Lindesnes, Norway (58°N) [*Telegadas*, 1971; *Nydal and Lövseth*, 1983]. At all these stations, the phase of the $\Delta^{14}C$ seasonal cycle was similar, reaching a maximum in mid and late summer, and a minimum in mid winter. Further to the south, a seasonal cycle with similar amplitude and phase existed during this period at Rehovoth, Israel (32°N), Izana, Tenerife Island, Spain (28°N), and Mas Palomas, Grand Canary Island, Spain (27°N) [*Nydal and Lövseth*, 1983]. These extensive surface observations and those from aircraft [*Telegadas*, 1971] provide evidence that the seasonal cycle of $\Delta^{14}C$ was coherent and widespread in the Northern Hemisphere troposphere in the mid and late 1960s, but became more subtle with time. As suggested by *Broecker and Peng* [1994], the damping of this seasonal cycle may serve as a constraint on changes in the stratospheric ^{14}C inventory.

[6] In later decades, stations in the Northern Hemisphere that were most exposed to fossil fuels tended to show larger seasonal amplitudes than those that were more remote [*Levin et al.*, 1989, 1995; *Meijer et al.*, 1995]. For example, during the 1980s the peak to trough amplitude of $\Delta^{14}C$ measured at the surface near Groningen, the Netherlands was approximately 30‰, whereas at Izana in the Canary Islands, the amplitude was only 5‰ [*Meijer et al.*, 1995]. Combining monthly $\Delta^{14}C$ and radon measurements, *Levin et al.* [1995] showed that fossil fuels emissions in Europe may have a seasonality that is substantially greater than that predicted by economic analyses of fuel use.

[7] In the tropics where fossil fuel effects are greatly reduced, large seasonal variations in $\Delta^{14}C$ were observed in the early 1990s (∼40‰) that may have been caused by changes in ocean upwelling strength during an El Nino event [*Rozanski et al.*, 1995]. At Wellington, New Zealand, *Manning et al.* [1990] observed a decrease in the seasonal cycle of $\Delta^{14}C$ from 1966 to 1980 and then a reversal of the phase and an increase in amplitude from 1980 to 1988. Model analyses of stratosphere-troposphere exchange could not explain this phase reversal, leaving open the possibility of ocean or land contributions [*Manning et al.*, 1990].

[8] Measurements from Europe over the last 2 decades provide evidence for a strong continental Suess Effect, with fossil fuels driving down the mean annual $\Delta^{14}C$ by over 20‰ in the European interior as compared with marine stations at similar latitudes [*Levin and Hesshaimer*, 2000; *Meijer et al.*, 1995]. Measurements from *Levin and Hesshaimer* [2000] provide evidence for a distinct latitudinal profile during the early 1990s with a minimum in mean annual $\Delta^{14}C$ at mid latitudes in the Northern Hemisphere from fossil fuels, (∼−3‰), a maximum near the equator (∼+2.5‰), and a second minimum near 60°S (∼−3.0‰) caused by exchange with the Southern Ocean. This profile is markedly different from model projections of the preindustrial latitudinal profile that had atmospheric minimums in northern high latitudes and southern high latitudes, and a Southern Ocean to equator difference of over 7‰ [*Braziunas et al.*, 1995].

[9] Using an atmospheric tracer model, here we explore the seasonal and latitudinal variability of $\Delta^{14}C$ since the 1960s. A primary objective of our analysis was to develop a predictive understanding of fossil, ocean, stratosphere, and terrestrial biosphere contributions to $\Delta^{14}C$ to more fully take advantage of past and future observations of this tracer. We also report experimental evidence from a transect of sites across Alaska that confine the range of possible carbon residence times in northern terrestrial ecosystems and con-

sequently their contemporary impact on atmospheric $\Delta^{14}C$. Building on our analysis that isolated individual processes, we predict that several features of the latitudinal profile of atmospheric $\Delta^{14}C$ will change over the duration of the 21st century.

2. Methods

[10] We made separate atmospheric model runs for fossil fuel, ocean, terrestrial biosphere, and stratosphere fluxes of CO_2 and $^{14}CO_2$. We focused on the period from 1960 to 1990 when long-term records from Fruholmen, Norway [*Nydal and Lövseth*, 1996] and Wellington, New Zealand [*Manning et al.*, 1990] allowed us to evaluate model scenarios. We also describe measurements of soil respiration $\Delta^{14}C$ from tundra and boreal forest sites in Alaska.

[11] For our atmospheric model runs, we used pulse response (or Green's) functions from a three-dimensional (3-D) atmospheric general circulation tracer model. We made the pulse-response functions by releasing a gaseous "dye" tracer into the atmospheric model at a constant rate from a particular region (Table 2) for short interval of time (1 month). We then tracked the 3-D pattern of emitted tracer until it was well mixed (over a period of 3 years). In the model simulations described below, we combined and scaled these pulse functions according to the intensity of $^{14}CO_2$ or $^{12}CO_2$ fluxes in each region. In this way, we constructed atmospheric distributions of $\Delta^{14}C$ that were consistent with our estimates of sources and sinks.

[12] The advantage of the pulse-response approach is that it is computationally efficient: the atmospheric model has to be run only once to generate the pulse functions. This efficiency enables the analysis of multiple atmospheric model scenarios, each lasting over a period of several decades in the post bomb era. Using the pulse-response approach, it is possible to reproduce large-scale latitudinal and seasonal patterns of tropospheric CO_2 and $\delta^{13}CO_2$ [*Gurney et al.*, 2002; *Randerson et al.*, 2002], even though the approach largely neglects variability in fluxes within basis regions (i.e., there are only ~20 discrete units interacting with the atmosphere with this approach, as compared with a fully coupled biosphere-atmosphere model that may have 20,000).

2.1. Atmosphere Model

[13] We generated pulse-response functions from the coarse resolution Goddard Institute for Space Studies (GISS) atmospheric transport model [*Fung et al.*, 1991]. This version of the GISS tracer model has an 8° × 10° horizontal resolution, nine vertical levels, and uses the same winds and circulation statistics as a higher resolution (4° × 5°) atmospheric model [*Tans et al.*, 1990]. The atmospheric tracer model uses 4-hour wind fields, and operates with a 1-hour time step. We directly compared the lowest level of the model with surface observations; this level had a thickness of ~50 mb and extended from the surface to 949 mb, or ~400 m.

[14] We constructed the atmospheric pulse functions by separately running the GISS tracer model for 36 months with an arbitrary initial pulse of 1 Pg C/month in each basis region listed in Table 2. Geographically, the fluxes used to generate the pulse were distributed evenly within each basis region for the case of the oceans and stratosphere, according to the spatial distribution of annual NPP for land [*Randerson et al.*, 1997], and according to 1° × 1° maps of emissions [*Andres et al.*, 1996] for fossil fuels.

Table 2. Basis Regions Used to Generate Atmospheric Pulse Functions

Region	Location
Land	
1. North America (High Latitudes)	North of 56°N
2. Eurasia (High Latitudes)	North of 56°N
3. North America (Midlatitudes)	40°N to 56°N
4. Eurasia (Midlatitudes)	40°N to 56°N
5. North America (Low Latitudes)	24°N to 40°N
6. Eurasia (Low Latitudes)	24°N to 40°N
7. Sub-Tropics and Tropics N.H.	0°N to 24°N
8. Southern Hemisphere Land	0°S to 56°S
Ocean	
9. North Atlantic (High Latitude)	North of 40°N
10. North Pacific (High Latitude)	North of 40°N
11. North Atlantic (Low Latitude)	0°N to 40°N
12. North Pacific (Low Latitude)	0°N to 40°N
13. South Atlantic	0°S to 48°S
14. South Pacific	0°S to 48°S
15. Indian Ocean	16°N to 48°S
16. Southern Ocean	South of 48°S
Stratosphere (at 200 mb)	
17. Northern Hemisphere High Latitudes	North of 60°N
18. Northern Hemisphere Midlatitudes	30°N to 60°N
19. Southern Hemisphere Midlatitudes	30°S to 60°S
20. Southern Hemisphere High Latitudes	South of 60°S
Fossil Fuels	
21. 1990 Spatial Map From *Andres et al.* [1996]	All Land

[15] The impact of surface and stratosphere carbon fluxes on troposphere $\Delta^{14}C$ depends strongly on background troposphere ^{14}C and CO_2 levels. For example, in the absence of other exchange, a 6 Pg C/yr fossil fuel flux in 1990 caused a decrease in $\Delta^{14}C$ of 9.2‰ (in an atmosphere of 355 ppm and 145‰) whereas the same flux in a future atmospheric scenario of 500 ppm and −60‰ [*Caldeira et al.*, 1998] would lead to a decrease of only 5.3‰. In the extreme, a flux has no impact on the isotopic composition of the atmosphere when its composition is equal to that of the background atmosphere. To capture these effects on $\Delta^{14}C$ in our global model, we adjusted the annual mean background levels of CO_2 and $^{14}CO_2$ to match a global mean time series of observations (section 2.2). We then added the cumulative effect of atmospheric fluxes from the previous 36 months (including the current time step) using the Green's functions described above. We assumed that fluxes that occurred 36 months or more prior to the current model time step did not contribute to spatial or temporal gradients of troposphere $\Delta^{14}C$ (i.e., these fluxes were well mixed and contributed only to the background).

[16] We started our atmospheric model runs in 1955, and then started our analysis of seasonal and spatial trends in the early 1960s. This allowed the troposphere a period of over 3 years to adjust to modeled surface fluxes. As described below, our flux models of the ocean, terrestrial biosphere, and stratosphere were initialized and forced with data from

periods well before the tropospheric tracer model runs began in 1955.

2.2. Atmospheric $\Delta^{14}C$ Record

[17] We constructed a smoothed atmospheric $\Delta^{14}C$ record using a spline fit [*Enting*, 1987] to observations from *Stuiver et al.* [1998] and *Nydal and Lövseth* [1996] for the period of 1700 to 1994, and from 1994 to 2000 based on an atmospheric model scenario from *Caldeira et al.* [1998] in which fossil fuel emissions were prescribed following the IPCC IS92a "business-as-usual" scenario.

[18] We compared our model results with seasonal observations from two stations: Fruholmen, Norway (71°N, 24°E) [*Nydal and Lövseth*, 1996] and Wellington, New Zealand (41°S, 175°E) [*Manning et al.*, 1990]. To isolate seasonal variations in these two records, we removed the long-term secular trend using a smoothing spline [*Enting*, 1987]. The residual was used to construct seasonal cycles by grouping all the observations into 2-month intervals. Standard deviations were calculated using all the observations within each interval.

2.3. Fossil Fuel Fluxes

[19] We modeled monthly fossil fuel emissions using a sine function with a maximum in January and a minimum in July, and a peak to trough amplitude of 30%. This seasonality is consistent with the analysis by *Rotty* [1987] for northern regions including Europe, Russia, Canada, the U.S. and Japan during the early 1980s [*Randerson et al.*, 2002]. It is difficult to justify constructing a more complicated fossil fuel scenario due to the paucity of seasonal fossil fuel emissions data. Annual total emissions from 1955 to 2000 were taken from *Marland et al.* [2000]. We prescribed the spatial distribution of fossil fuels in our single fossil basis function from the $1° \times 1°$ maps constructed by *Andres et al.* [1996] for 1990.

2.4. Ocean Fluxes

[20] We used monthly ocean-atmosphere and atmosphere-ocean fluxes of $^{14}CO_2$ and CO_2 from the Lawrence Livermore National Laboratory (LLNL) three-dimensional ocean circulation model in our analysis [*Duffy and Caldeira*, 1995; *Duffy et al.*, 1997]. Atmospheric $\Delta^{14}C$, winds, and natural and preindustrial radiocarbon spin up followed the protocol of the Ocean Carbon Model Intercomparison Project (OCMIP; http://www.ipsl.jussieu.fr/OCMIP/phase2/) [*Orr et al.*, 2001]. Seasonal changes in the $^{14}CO_2$ flux from the ocean to the atmosphere arise from month-to-month changes in the gross sea to air CO_2 flux and from month-to-month changes in the $\Delta^{14}C$ composition of the mixed layer (Figure 1). Monthly fluxes from the LLNL ocean model were averaged over eight regions for use with our atmospheric pulse functions (Table 2). The LLNL ocean model simulation used here in our troposphere analysis ended in 1990.

2.5. Stratosphere Fluxes

[21] Most of the large nuclear fireballs (from detonations at the surface or in the free troposphere) were lifted across the tropopause and into the lower stratosphere [*Glasstone and Dolan*, 1977]. The version of the GISS model we used here had nine vertical levels and did not have a well-defined

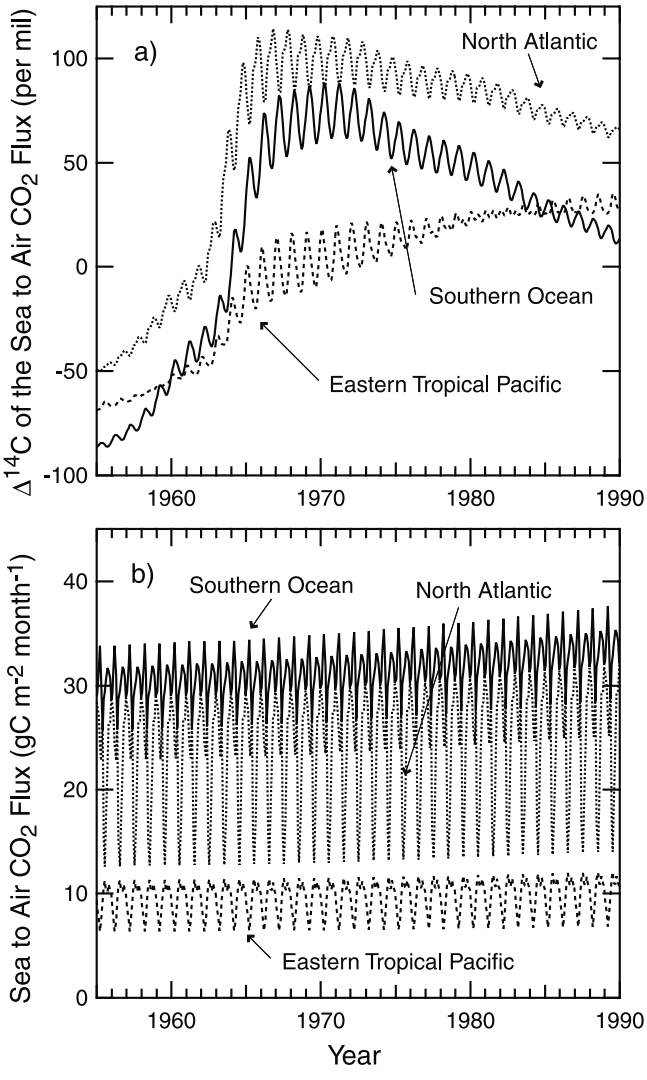

Figure 1. The ocean to atmosphere ^{14}C flux from the LLNL 3-dimensional ocean model had a seasonal cycle arising from two related factors: a) changes in the mixed layer $\Delta^{14}C$ (caused partially by month-to-month changes in upwelling strength) and b) changes in the sea to air CO_2 flux (caused partially by month-to-month changes in winds). In the North Atlantic (dotted lines; north of 40°N) the magnitude of the sea to air flux increased from summer to winter, having a substantial impact on $^{14}CO_2$ exchange. In the eastern tropical Pacific (dashed lines; 5°N to 5°S and 120°W to 88°W), and in the Southern Ocean (solid lines; South of 48°S) seasonal changes in mixed layer $\Delta^{14}C$ also played a key role. In the eastern tropical Pacific, the $\Delta^{14}C$ of the mixed layer reversed seasonal phase in the early 1980s because upwelling became more enriched than surrounding surface waters. The reason for this reversal is that upwelling water in the ventilated thermocline circulation was at the surface several decades earlier, and partially equilibrated with the very high atmospheric levels in the 1960s and 1970s. The LLNL ocean model predicted seasonal variations in Southern Ocean mixed layer $\Delta^{14}C$ that exceeded 25‰ during the late 1960s and early 1970s.

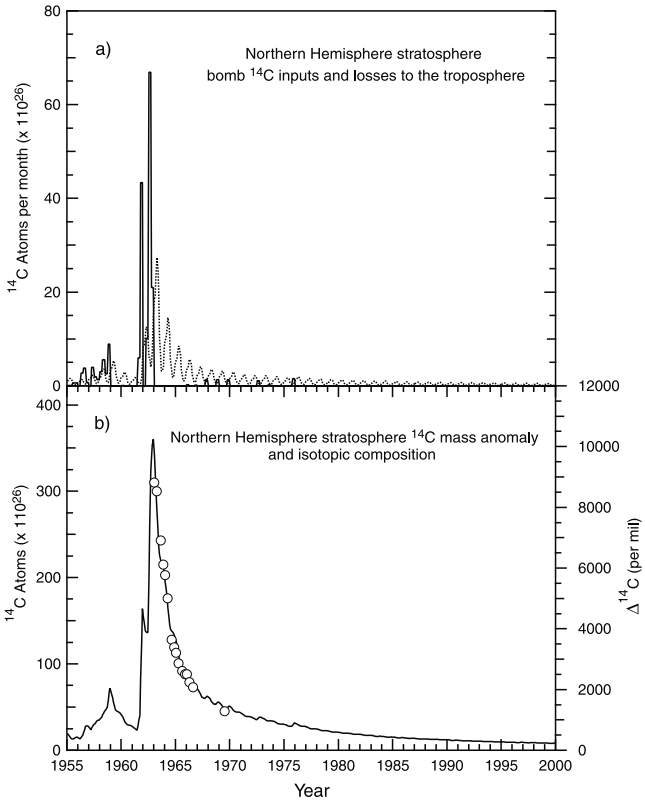

Figure 2. (a) Northern Hemisphere stratosphere model inputs from bomb ^{14}C (solid line) and losses from extratropical stratosphere-troposphere exchange (dotted line). Units are in radiocarbon units (RCUs), where 1 RCU is equal to 1×10^{26} atoms of ^{14}C. Output fluxes (arising from bomb, tropospheric entrainment, and cosmogenic ^{14}C sources) from the stratosphere model were injected into the GISS atmospheric model at 200 mb using pulse response functions described in the text. Hydrogen bomb tests in the early 1960s in the Northern Hemisphere accounted for the majority of bomb produced $\Delta^{14}C$ (Table 1). (b) The ^{14}C anomaly in the Northern Hemisphere stratosphere decreased in late 1960s, consistent with observations from *Telegadas* [1971] (circles). From 1970 to 2000, stratosphere ^{14}C decreased much more slowly, as tropospheric re-entrainment and cosmogenic production became the dominant ^{14}C sources. The ^{14}C anomaly was defined as the ^{14}C above that expected when the $^{14}C/^{12}C$ ratio was equal to $R_{standard}$ (where $R_{standard}$ is defined as 1.176×10^{-12}).

stratosphere. We simulated stratosphere-troposphere exchange by creating separate box models for the Northern and Southern hemisphere stratosphere, each with monthly inputs from bomb radiocarbon [*Enting*, 1982], cosmogenic production, and entrainment of tropospheric air (representing upward flow in the tropics), and monthly losses (representing net stratosphere-troposphere mixing outside of the tropics) (Figure 2a). Stratospheric losses were evenly distributed in the GISS atmospheric tracer model in regions poleward of 30° using pulse functions at 200 mb (Table 2).

[22] The total inventory of bomb ^{14}C released into the tracer model was 625 radiocarbon units (1 RCU = 1×10^{26} atoms ^{14}C) through 1975 (Table 1 and Figure 2). Bomb inputs consisted of detonation strength estimates (in Mt TNT) corrected for the height of detonation (and thus interception of neutrons by the surface instead of by atmospheric N) [*Enting*, 1982]. We used a conversion factor of 1.35 RCUs/Mt TNT to estimate bomb-produced ^{14}C [*Lassey et al.*, 1996]. Nuclear explosions in the Northern hemisphere entered the Northern hemisphere stratosphere, while explosions in the Southern hemisphere entered the Southern hemisphere stratosphere according to detonation sites provided by *Enting* [1982]. We did not allow mixing in the stratosphere across the equator; the Northern and Southern Hemisphere stratosphere box models were isolated from each other.

[23] Cosmogenic ^{14}C production has been estimated at about 2.3 to 2.5 RCUs/yr [*Lingenfelter*, 1963]. We uniformly distributed this flux in the Northern and Southern Hemisphere stratosphere models. While cosmogenic ^{14}C production represents a relatively small perturbation when compared with bomb inputs and fossil fuel dilution over the last few decades, it is becoming an increasingly important factor in determining the global decrease in atmospheric $\Delta^{14}C$ [*Caldeira et al.*, 1998]. We neglected ^{14}C production from nuclear power plants, which was less than 0.5 RCUs/yr in 1990 [*Hesshaimer et al.*, 1994].

[24] Each stratospheric box model had a lower and upper reservoir. In the Northern Hemisphere, these reservoirs were assigned residences times of 1.5 years and 5 years based on measurements of CO_2 and N_2O by *Andrews et al.* [2001]. Bomb inputs and upward troposphere fluxes entered the lower stratosphere reservoir, where they could either move into the upper stratosphere or vent directly into the extratropical troposphere (and thus into the GISS atmosphere model via the pulse response functions previously described). The lower and upper model reservoirs accounted for 78% and 22% of the stratosphere mass, respectively. With the two-reservoir stratosphere model used here, we were able to fit Northern Hemisphere stratosphere observations from *Telegadas* [1971] (Figure 2b). With a 1-box stratosphere model (data not shown) it was difficult to reproduce this time series; modeled ^{14}C decreased more rapidly than the observations in the late 1960s. The southern stratospheric model was identical to the northern one, but incoming and outgoing fluxes from the troposphere were reduced by 40% [*Gettelman and Sobel*, 2000]. The tropospheric air entrained into the stratosphere was assumed to have equal contributions from Northern and Southern hemispheres [*Boering et al.*, 1996].

[25] We used seasonal estimates of the net stratospheric flux into the extratropical troposphere following the mass budget method developed by *Appenzeller et al.* [1996]. This seasonal distribution [*Appenzeller et al.*, 1996, Figure 8] had a maximum in April and May (Figure 3) in the Northern Hemisphere and allowed us to approximately capture the phase of the seasonal cycle of $\Delta^{14}C$ observed at Fruholmen, Norway, and Wellington, New Zealand. With other seasonal distributions of extra tropical (Northern Hemisphere) cross tropopause flux (CTF) that peaked in mid winter [i.e, the

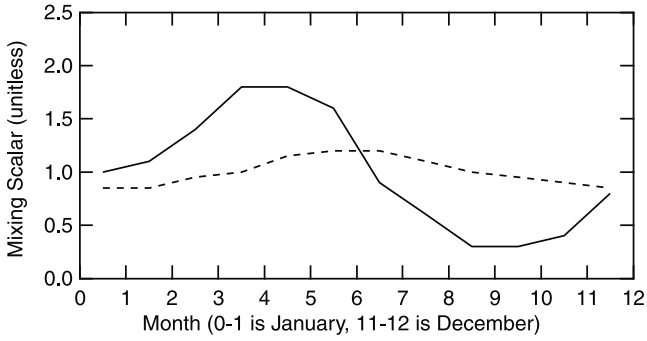

Figure 3. Stratospheric fluxes were injected into the upper troposphere of the GISS atmospheric model at 200 mb with a seasonal distribution shown here (based on estimates of net cross tropopause flux (CTF) described by *Appenzeller et al.* [1996]). The Northern Hemisphere mixing scalar is represented with a solid line, and Southern Hemisphere mixing scalar with a dashed line. Stratospheric fluxes were released at the 200 mb level in the GISS model, and uniformly from 30° to the pole. Each scalar had a mean annual value of 1.

gross fluxes as estimated using the Wei method as reported in *Gettelman and Sobel*, 2000], we were unable to match the seasonal dynamics of the surface $\Delta^{14}C$ observations.

2.6. Terrestrial Biosphere Fluxes

[26] We divided the land surface into eight regions (Table 2). In each region, terrestrial biosphere-atmosphere CO_2 exchange was calculated as the approximate balance between net primary production (NPP) and heterotrophic respiration following a simple carbon model described by *Randerson et al.* [2002]. We estimated monthly NPP from the product of absorbed photosynthetically active radiation (APAR) and a globally uniform light use efficiency term. APAR was calculated for each region using satellite-derived vegetation indices (Advanced Very High Resolution Radiometer Simple Ratio) [*Los et al.*, 1994] and solar insolation [*Bishop and Rossow*, 1991]. In the simulations presented here, we used a globally uniform light use efficiency of 0.52 g C/MJ PAR (which yielded a global annual NPP of 60 Pg C/yr). A simple description of carbon cycling and heterotrophic respiration within each region included a fixed plant allocation scheme and a temperature-dependent rate of microbial decomposition in litter and soil carbon pools. Allocation to leaves, fine roots, and wood had a fixed proportion of 0.4, 0.4, and 0.2. A Q10 of 1.6 described the sensitivity of heterotrophic respiration to mean monthly air temperature in each basis region. We neglected plant respiration in our model because we assumed it had a residence time much less than 1 year and thus imparted only a small isotopic anomaly to CO_2 in the local atmosphere.

[27] The combination of the light use efficiency and Q10 values used here yielded realistic descriptions of the phase and amplitude of the seasonal cycle of CO_2 and $\delta^{13}CO_2$ at mid and high latitude NOAA/CMDL stations in the Northern Hemisphere (Figure 4). For all terrestrial biosphere scenarios presented below, we assumed that NPP remained in annual steady state at 60 Pg C/yr. The biosphere and atmospheric models were coupled so that isotopic fluxes in one region affected atmospheric composition and consequently isotope fluxes in downwind regions at later times [*Randerson et al.*, 2002]. Soil and vegetation carbon pools in the terrestrial model were allowed to reach ^{14}C steady state in 1750. From 1750 until the start of the atmospheric model runs in 1955, the $\Delta^{14}C$ of NPP was forced to match the observed atmospheric record (section 2.2) in all basis regions. During each time step of the atmospheric model, carbon uptake by the terrestrial biosphere model had a prescribed $\Delta^{14}C$ value from the atmospheric mean over the same basis region in the previous time step.

[28] We created three terrestrial biosphere scenarios by multiplying the turnover time of all the carbon pools in our model by a factor of 0.5, 1.0, or 2.0 (Table 3). We created these scenarios because terrestrial carbon residence times are relatively uncertain, and this range spanned previous

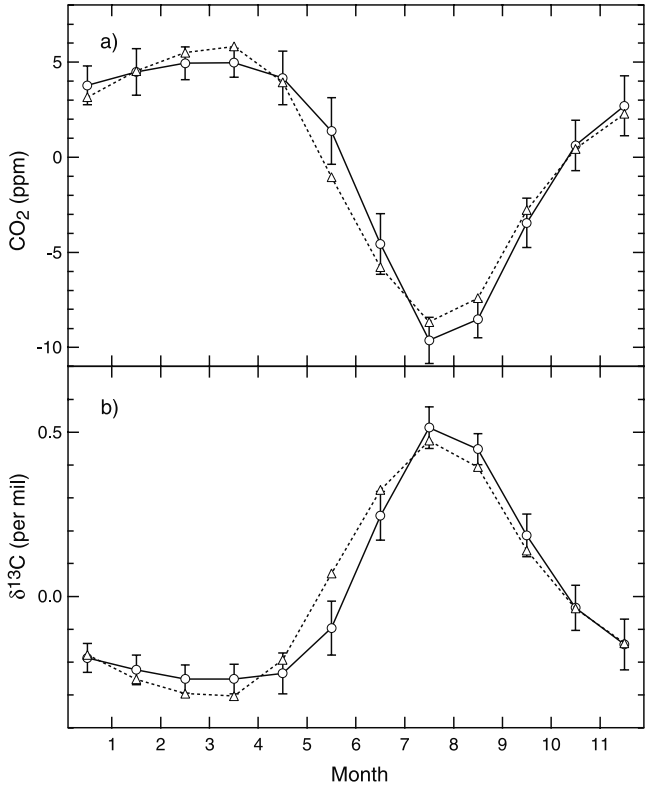

Figure 4. (a) The mean seasonal cycle of CO_2 at NOAA/CMDL stations north of 50°N from 1993 to 1997 was primarily caused by net CO_2 fluxes from terrestrial ecosystems with small contributions from fossil fuel and ocean exchange (solid lines, standard deviation error bars) [*Randerson et al.*, 2002]. The combination of light use efficiency and Q10 values used here captured most of phase and amplitude of the Northern Hemisphere seasonal cycle (dotted line). (b) Same as (a) but for $\delta^{13}CO_2$. Measurements are from the INSTAAR and NOAA/CMDL observation stations used in the analysis by *Randerson et al.* [2002]. Plant discrimination against ^{13}C was set at 19‰ in the terrestrial ecosystem model.

Table 3. Terrestrial Biosphere Model Carbon Cycling Scenarios

Terrestrial Biosphere Scenario	MRT of the Boreal Forest North of 40°N, years	MRT of the Terrestrial Biosphere, years	Crossover Year (When $\Delta^{14}C_{Rh} = \Delta^{14}C_{atm}$)[a]	Maximum Seasonal $\Delta^{14}C$ Amplitude 1965, ‰[b]	Maximum Seasonal $\Delta^{14}C$ Amplitude 1990, ‰
1.	22	13	1984	24.1	2.3
2.	43	24	1990	30.3	1.0
3.	85	48	1991	35.5	0.5

[a] For regions north of 40°N.
[b] The global maximum amplitude from the surface layer of the GISS atmospheric tracer model.

estimates of ^{14}C uptake by the terrestrial biosphere between 1965 and 1990 (Table 4). In the context of these scenarios, it is worth noting that while field measurements and satellite data provide a strong global constraint on NPP [*Running et al.*, 1999], comparable global constraints on carbon residence times are relatively weak. It is doubtful the terrestrial biosphere isotopic disequilibrium forcing for $\delta^{13}C$ or $\delta^{14}C$ is known within a factor of 4 because this term critically depends on processes such as fine root allocation, mortality, and decomposition and only weakly on the mass of carbon in soils and vegetation [*Trumbore*, 2000]. Many of these processes are not well understood or well represented in models at regional and global scales that are used for disequilibria estimates. In our analysis of the combined processes, we used scenario 1 from the terrestrial biosphere because this scenario most closely matched a recent estimate (Table 4) that used satellite and climate data as constraints on the spatial distribution of NPP and decomposition across ecosystems with a $1^\circ \times 1^\circ$ spatial resolution [*Thompson and Randerson*, 1999].

[29] Since our analysis focused on $\Delta^{14}C$, we did not consider the effects of mass dependent fractionation (against ^{13}C or ^{14}C). If we had considered $\delta^{14}C$, the seasonal amplitude arising from fractionation during photosynthesis would have added a seasonal cycle with an amplitude of ~1.5‰ at mid and high northern latitudes, approximately double that observed for $\delta^{13}C$ [*Trolier et al.*, 1996].

2.7. Soil Respiration $\Delta^{14}C$ Measurements

[30] Soil respiration and surface atmosphere $\Delta^{14}C$ measurements were made at midday during July 2000 across a latitudinal transect in Alaska. Two sites were located in mature black spruce forest in interior Alaska, at the Caribou Poker Creek Research Watershed (65°07′N, 147°20′W, elevation ~500 m), part of the Bonanza Creek Long Term Ecological Research (BNZ-LTER) site, and at Delta Junction, Alaska (63°55′N, 145°22′W, elevation ~400 m). The third site was located in tussock tundra at the Toolik Lake LTER on the North Slope of the Brooks Range (68°38′N, 149°43′W, elevation 760 m).

[31] Soil respiration $^{14}C/^{12}C$ and $^{13}C/^{12}C$ isotopic ratios were measured using a modified dynamic flow chamber system [*Gaudinski et al.*, 2000]. Air was drawn from chambers mounted on collars that had been permanently installed in the soil surface, through an infrared gas analyzer to determine the CO_2 concentration, and then either through a soda lime CO_2 scrubber or through a molecular sieve before returning to the chamber. To collect respired CO_2 alone, CO_2 was first scrubbed with soda lime from the chamber system to remove background atmospheric air. Scrubbing was maintained until the equivalent of 2–3 chamber volumes of air had passed through the scrubber. The airstream was then diverted through a molecular sieve that quantitatively trapped CO_2 until 1.0–1.5 mg of CO_2-C was adsorbed. Atmospheric samples were collected on molecular sieves using the same system, except that the air intake was placed above ground at a height of 2 m. Atmospheric samples were collected at the Toolik Lake and Delta sites. In the laboratory, the molecular sieve traps were heated to 675°C, which desorbs CO_2 [*Bauer et al.*, 1992]. Carbon dioxide was then cryogenically purified on a vacuum line, sub sampled for $\delta^{13}C$ analysis, and reduced to graphite using titanium hydride, zinc, and a cobalt catalyst [*Vogel*, 1992]. Graphite targets were sent to the LLNL Center for Accelerator Mass Spectrometry (LLNL-CAMS) for $\Delta^{14}C$ analysis. The $^{13}C/^{12}C$ isotopic ratios were used in the final analysis to correct the $^{14}C/^{12}C$ ratios for discrimination by photosynthesis [*Stuiver and Polach*, 1977], and to correct for remaining atmospheric CO_2 in the chamber-sampler system.

3. Results

[32] In this section, we first present model results for the individual processes. We then compare our combined model time series with observations from Fruholmen, Norway, and Wellington, New Zealand. Finally, we report soil respiration $\Delta^{14}C$ measurements from tundra and boreal forest ecosystems in Alaska that help constrain the atmospheric $\Delta^{14}C$ signal driven by northern terrestrial ecosystems.

3.1. Fossil Fuels

[33] The amplitude of the fossil fuel component did not substantially increase from 1965 to 1990 (Figures 5a and 6a). While total fossil fuel emissions almost doubled during this period, from 3.1 Pg C/yr in 1965 to 6.1 Pg C/yr in 1990 (a 49% increase) [*Marland et al.*, 2000],

Table 4. Estimates of Terrestrial Biosphere ^{14}C Uptake From 1965 to 1990[a]

Reference	Biosphere Radiocarbon Storage From 1965 to 1990, $\times 10^{26}$ atoms ^{14}C
Siegenthaler and Joos [1992]	99
Jain et al. [1996]	92
Hesshaimer et al. [1994]	60
Broecker and Peng [1994]	39
Thompson and Randerson [1999]	33
This study: Scenario 1.	42
This study: Scenario 2.	89
This study: Scenario 3.	125

[a] Table modified from *Jain et al.* [1996].

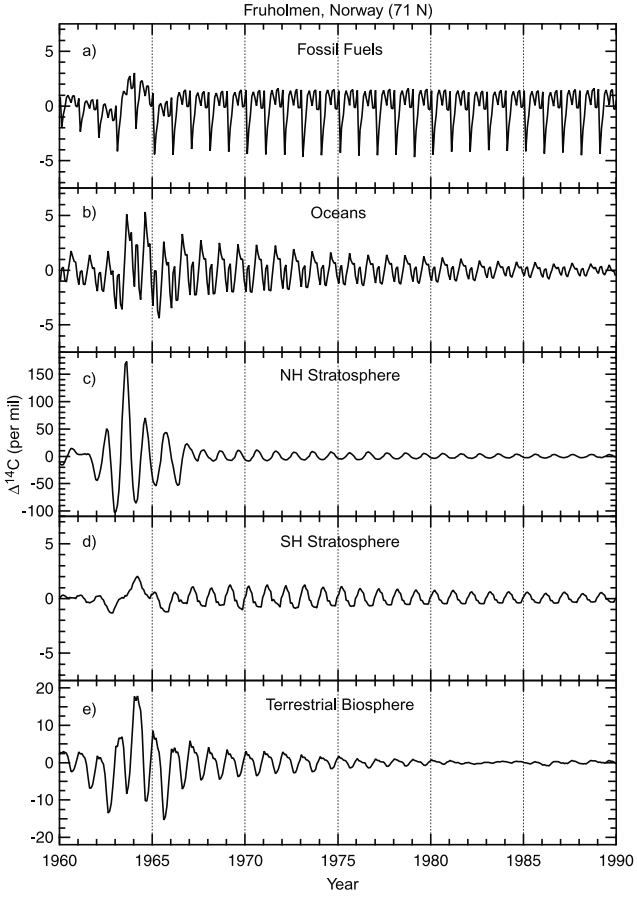

Figure 5. Components of the $\Delta^{14}C$ seasonal cycle at Fruholmen, Norway (71°N, 13°E) caused by (a) fossil fuels, (b) ocean exchange, (c) Northern Hemisphere stratosphere exchange, (d) Southern Hemisphere stratosphere exchange and (e) terrestrial biosphere fluxes (scenario 1). The long-term atmospheric trend was removed using a smoothing spline. Model estimates presented here and in all subsequent figures were taken from the surface layer of the GISS atmospheric tracer model.

atmospheric $\Delta^{14}C$ decreased by almost the same amount, from 800‰ to 160‰ [*Nydal and Lövseth*, 1996]. This change in $\Delta^{14}C$ corresponds to a 64% decrease in the ^{14}C to ^{12}C ratio of atmospheric CO_2. Concurrently, atmospheric CO_2 increased from 665 to 760 Pg C over this period (an 11% increase) [*Keeling et al.*, 1989]. The increasing atmospheric CO_2 mass and the decreasing ^{14}C to ^{12}C ratio of atmospheric CO_2 caused the relative impact of fossil fuels on $\Delta^{14}C$ to remain relatively constant. At Fruholmen, Norway, $\Delta^{14}C$ seasonal cycle arising from fossil fuels had a minimum in February (corresponding to the time when fossil fuel derived CO_2 concentrations were highest in the atmospheric model surface layer). The total peak-to-trough amplitude of the fossil fuel component was approximately 5‰ in 1990 (Figure 5a). At Wellington, New Zealand, the fossil fuel component was less than 1‰, with a maximum in March and a minimum in August, September, and October (Figure 6a).

[34] Fossil fuel CO_2 plumes created increased seasonal amplitudes and depleted mean annual $\Delta^{14}C$ values over Europe, the east coast of North America, and the east coast of Asia in 2000 (Figure 7). The $\Delta^{14}C$ seasonal amplitude from fossil fuel emissions reached a maximum over Eastern Europe at 12‰ (Figure 7a), and was slightly offset to the east and north from the minimum in mean annual $\Delta^{14}C$. Globally, the mean annual $\Delta^{14}C$ minimum occurred over Europe, with a value of −24‰ relative to the South Pole (Figure 7b).

[35] Despite relatively large fossil fuel fluxes from the west coast of North America, a large plume in $\Delta^{14}C$ was not evident over western North America in our model simulations. We only present spatial maps of the seasonal amplitude and mean annual gradient for the year 2000 because, as described above, the impact of fossil fuel emissions on $\Delta^{14}C$ did not rapidly change from the 1960s to the 1990s (Figure 5).

3.2. Oceans

[36] The ocean contribution to the $\Delta^{14}C$ seasonal cycle of atmospheric CO_2 was greatest in the mid 1960s when the air-sea differences in $\Delta^{14}C$ were large. At Fruholmen, peak-to-trough amplitudes in 1965 were approximately 9‰ in 1965, and decreased to approximately 1‰ in 1989 (Figure 5b). At Wellington, peak-to-trough ampli-

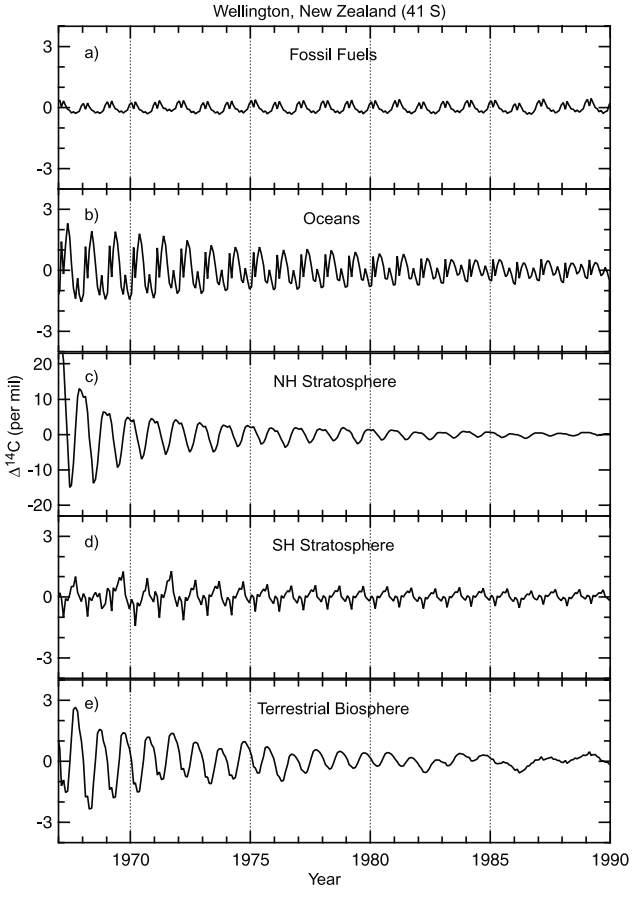

Figure 6. Same as Figure 5, but for the model grid cell that included Wellington, New Zealand (41°S, 175°E).

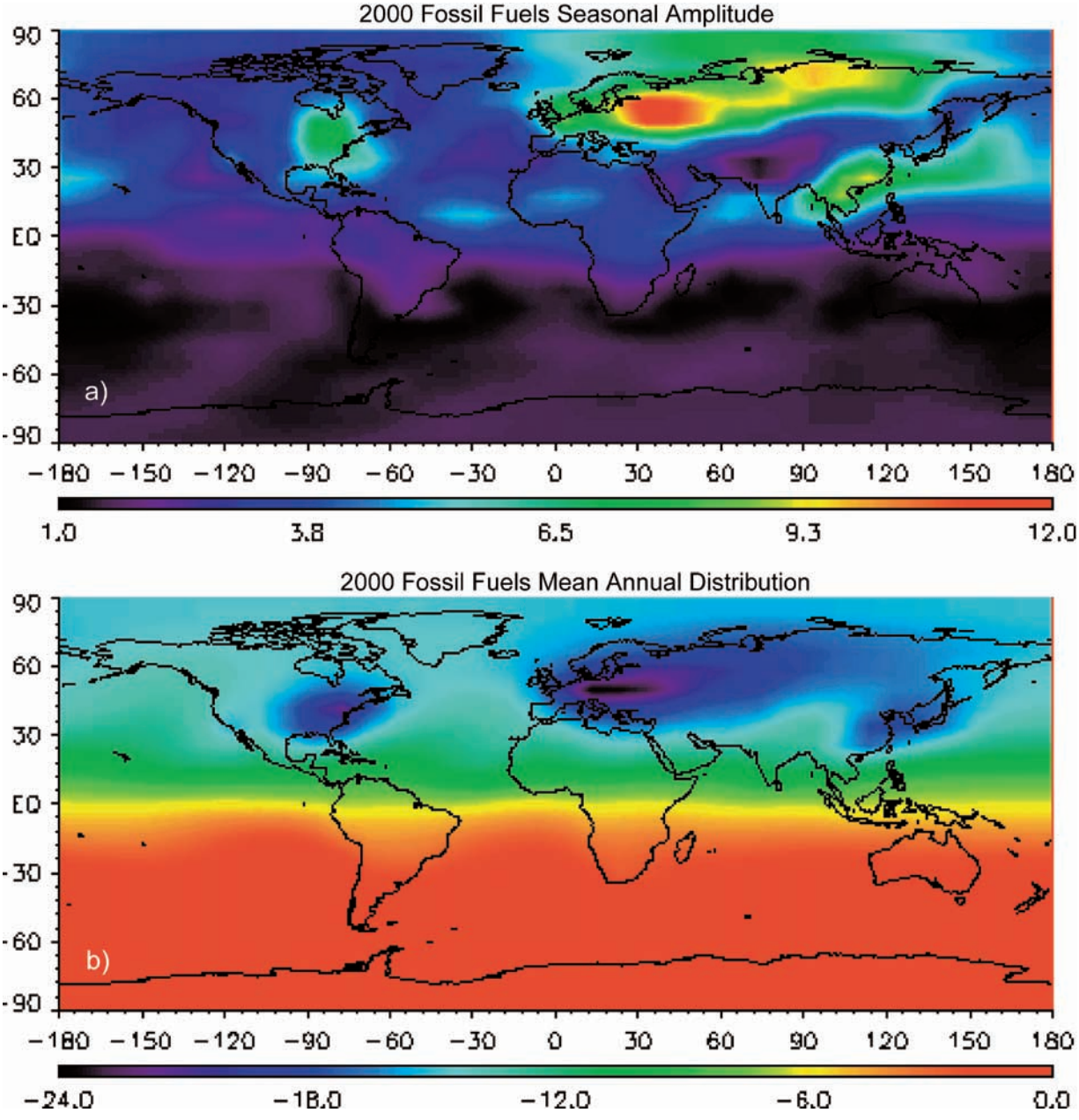

Figure 7. The contribution of fossil fuel emissions in 2000 to (a) the seasonal amplitude of $\Delta^{14}C$ and (b) the mean annual $\Delta^{14}C$ (relative to the South Pole).

tudes in the late 1960s were ~4‰ and decreased to less than 1‰ by 1989.

[37] The mean annual regional pattern of troposphere $\Delta^{14}C$ arising from ocean exchange changed substantially from 1965 to 1989 (Figure 8). In 1965, atmospheric $\Delta^{14}C$ anomalies over much of the ocean surface were relatively uniform (with the exception of the Southern Ocean and parts of the Arctic Ocean) and the land/sea contrast was large (Figure 8d). By 1989, the rapid equilibration of tropical oceans and mid-ocean gyres to relatively high tropospheric $\Delta^{14}C$ levels in previous decades led to a positive atmospheric $\Delta^{14}C$ anomaly in equatorial regions (Figure 8b).

[38] In the eastern tropical Pacific, upwelling from the wind driven circulation now had a higher $\Delta^{14}C$ content than surrounding surface waters, leading to a reversal of the seasonal cycle $\Delta^{14}C$ in ocean surface water (Figure 1). This reversal in the seasonal phase of surface water $\Delta^{14}C$ is consistent with coral measurements that show a rapid increase in the seasonal amplitude in the late 1960s and early 1970s, and then a decline in the late 1970s and early 1980s (as upwelling water became progressively more enriched) [*Guilderson and Schrag*, 1998; *Rodgers et al.*, 2000]. In contrast, upwelling with minimal bomb ^{14}C in the Southern Ocean continued to impart a negative $\Delta^{14}C$ anomaly to the atmosphere in this region (Figure 8b).

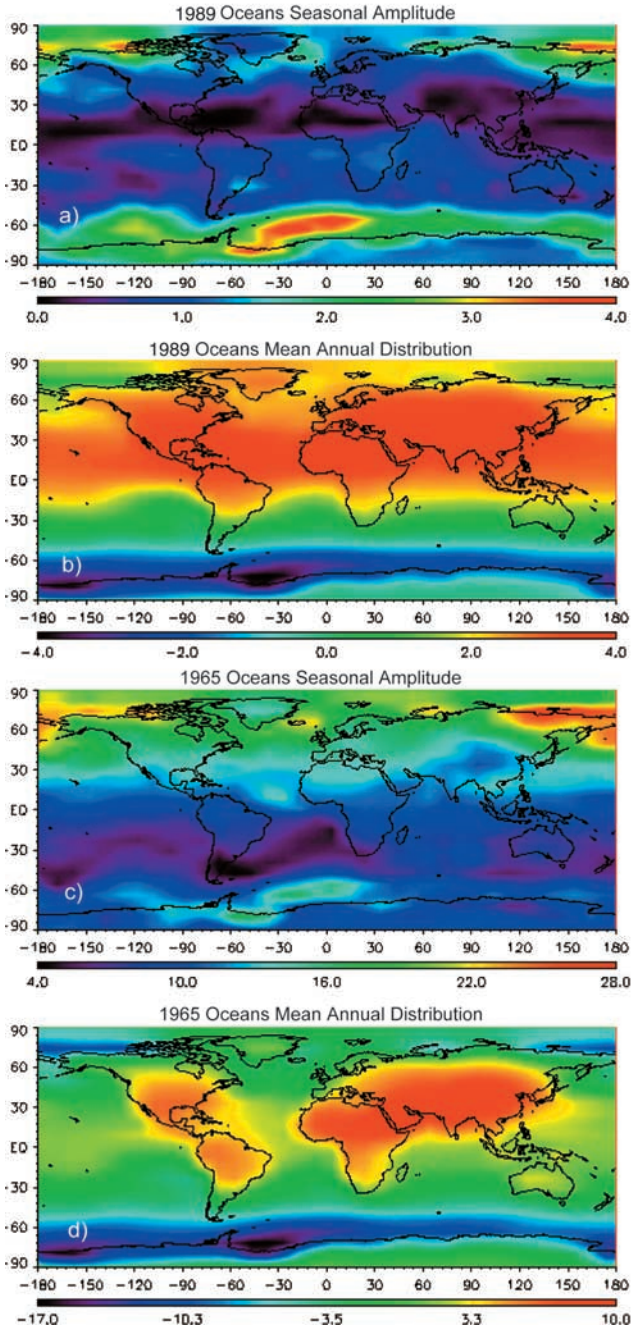

Figure 8. The contribution of ocean fluxes in 1989 to (a) the seasonal amplitude of $\Delta^{14}C$ and (b) the mean annual $\Delta^{14}C$ (relative to the South Pole). The same two maps are presented for 1965 (c and d). Ocean fluxes were from the LLNL three-dimensional ocean model. The mean annual $\Delta^{14}C$ values are relative to the South Pole and are from the lowest level of the atmospheric tracer model.

3.3. Stratosphere

[39] Northern Hemisphere stratosphere fluxes created seasonal amplitudes in excess of 250‰ in 1963 (Figure 5c). By 1970, the seasonal contribution had decreased to approximately 30‰. At Wellington, New Zealand, the seasonal amplitudes from the Northern hemisphere stratosphere were reduced by a factor of approximately 2 to 4 from those in the Northern Hemisphere during the late 1960s, and were delayed in phase by about 4–5 months (Figure 6c). During the 1960s, contributions from the southern stratosphere to the seasonal amplitudes at Fruholmen, Norway were small, in part because few nuclear detonations occurred in the Southern Hemisphere during this time (Figure 5d). At Wellington, fluxes from the Southern Hemisphere stratosphere were responsible for a seasonal amplitude of 2.5‰ in the late 1960s and ~1‰ in 1989.

[40] In 1965, almost the entire ^{14}C anomaly in the Northern Hemisphere stratosphere was a direct result of nuclear detonations (Table 5 and Figure 2). Over the following decade, almost all original bomb ^{14}C was flushed out of the stratosphere by atmospheric mixing and transport. By 1990, bomb ^{14}C accounted for less than 2.3% of the total ^{14}C anomaly in our modeled stratospheric flux (Table 5), and represented less than 0.05% of the original stratospheric ^{14}C anomaly in 1965 (Figure 2b). Despite the rapid flushing of this bomb ^{14}C, the stratosphere flux continued to play an important role in shaping the seasonal and latitudinal distribution of tropospheric $\Delta^{14}C$ during the 1970 to 2000 period. During this second stage, the primary mechanism enriching the stratospheric flux was the entrainment of tropospheric air in the tropics, and the time delay associated with its return via stratosphere-troposphere exchange in the extra-tropics. This time delay in our model led to an enrichment in the stratosphere flux because fossil fuels emissions and ocean exchange were concurrently decreasing tropospheric $\Delta^{14}C$ at the surface.

[41] When cosmogenic radiocarbon production was used as a sole input into our stratosphere model (no bomb inputs), we obtained a ^{14}C mass anomaly of 3.75 RCUs in the northern stratosphere, an upper stratosphere $\Delta^{14}C$ of 220‰, a lower stratosphere $\Delta^{14}C$ of 60‰, and a seasonal amplitude of ~1.3‰ at the surface at Fruholmen, Norway.

[42] With uniform cosmogenic production across both hemispheres (and a well mixed troposphere), our model generated no north-south gradient in tropospheric $\Delta^{14}C$. Reduced tropospheric exchange in the Southern Hemisphere stratosphere was compensated by the buildup of ^{14}C in the stratosphere, and thus higher $\Delta^{14}C$ levels in the extratropical flux. The reduced tropospheric exchange in the Southern Hemisphere stratosphere did, however, generate a

Table 5. Source of the ^{14}C Anomaly in the Northern Hemisphere Stratosphere Flux

	Percent Contribution From:[b]		
Year	Bomb ^{14}C[a]	Troposphere Uplift (Re-entrainment)	Cosmogenic Production
1965	95.5	3.8	0.7
1990	2.3	73.1	24.6
2000	0.6	60.8	38.6

[a] This refers to bomb ^{14}C originating from the initial nuclear detonation and fireball. ^{14}C that is entrained into the stratosphere by normal atmospheric circulation is included as tropospheric uplift.

[b] These percent contributions were estimated for the component of ^{14}C in the extratropical stratosphere to troposphere flux above a 0‰ baseline level (i.e., they represent the percent contribution to the ^{14}C mass above that expected for a carbon flux with a isotope ratio equal to $R_{standard}$, where $R_{standard}$ is equal to 1.176×10^{-12}).

north-south gradient when the troposphere was constrained to follow the observed post bomb trajectory, particularly during the 1970s and 1980s. More ^{14}C-enriched air circulated through the Northern Hemisphere stratosphere, creating a positive anomaly in northern latitudes. Even though $\Delta^{14}C$ levels were higher in the Southern Hemisphere stratosphere because of the longer residence times, this enrichment did not fully compensate for the reduction in the total stratosphere-troposphere flux in this hemisphere.

3.4. Terrestrial Biosphere

[43] During the 1960 to 2000 period, the terrestrial biosphere component of $\Delta^{14}C$ seasonal cycle reversed phase, with the timing of the phase transition depending on the residence times of carbon in the regions surrounding the observation station. In scenarios with relatively rapid carbon cycling (Table 3), the amplitudes of the initial post bomb seasonal cycle were relatively small and decayed more rapidly (Figure 9b) as compared with scenarios with relatively slow carbon cycling (Figures 9c and 9d). During this initial phase of the terrestrial biosphere response, the $\Delta^{14}C$ of respiration was much lower than the local atmosphere (Figure 9a). Consequently, respiration caused a decrease in $\Delta^{14}C$ near the surface during summer and fall, when respiration rates were high. As litter and soil pools equilibrated with post bomb atmospheric $\Delta^{14}C$ levels, the isotopic disequilibria between respiration and the atmosphere decreased, along with the terrestrial ecosystem contribution to the $\Delta^{14}C$ seasonal cycle.

[44] The terrestrial biosphere component of seasonal amplitude dropped to zero when the $\Delta^{14}C$ of heterotrophic respiration was equal to that of the local atmosphere. The timing of this phase transition depended on the residence time of carbon in nearby regions (Table 3). At observation stations closer to the equator than Fruholmen, Norway this phase transition occurred earlier, reflecting warmer temperatures and consequently more rapid carbon cycling within terrestrial ecosystems (data not shown).

[45] As heterotrophic respiration became more enriched than the local atmosphere, the terrestrial component of the seasonal cycle reversed phase, as compared with the initial post bomb terrestrial seasonal cycle. In this second stage, heterotrophic respiration was enriched in $\Delta^{14}C$ (relative to the local atmosphere), causing a positive anomaly at the surface in summer and fall, which was erased by atmospheric mixing during winter and spring. The disequilibrium between respiration and the atmosphere in the second stage was much smaller than in the first stage because the annual rate of change in global atmospheric $\Delta^{14}C$ had slowed. For the more rapid cycling scenarios, the seasonal amplitudes reached a maximum shortly after the phase transition time, whereas for the slow cycling time scenarios, the amplitudes continued to build out to the year 2000.

[46] The modeled effect of terrestrial ecosystem fluxes on the seasonal amplitude of $\Delta^{14}C$ was greatest over eastern Siberia and western North America (Figures 10a and 10c). Over the oceans, including sites such as Fruholmen, Norway, this effect was considerably weaker, both in 1965 and in 2000.

[47] Just as the terrestrial biosphere reversed phase in terms of its contribution to the seasonal cycle from 1965 to 2000, it also reversed its contribution to the mean annual latitudinal profile of $\Delta^{14}C$. In the year 2000, terrestrial biosphere fluxes (Scenario 1) caused a north-south atmospheric gradient of ~6‰, primarily because respiration from northern ecosystems was enriched relative to the contemporary atmosphere (Figure 10b). In contrast, in 1965, respiration from northern ecosystems had a $\Delta^{14}C$ content that was depleted by several hundred per mil as compared to the troposphere (Figure 9a). This large isotopic disequilibrium created a north-south difference of approximately −40‰ (Figure 10d). Without terrestrial exchange, the

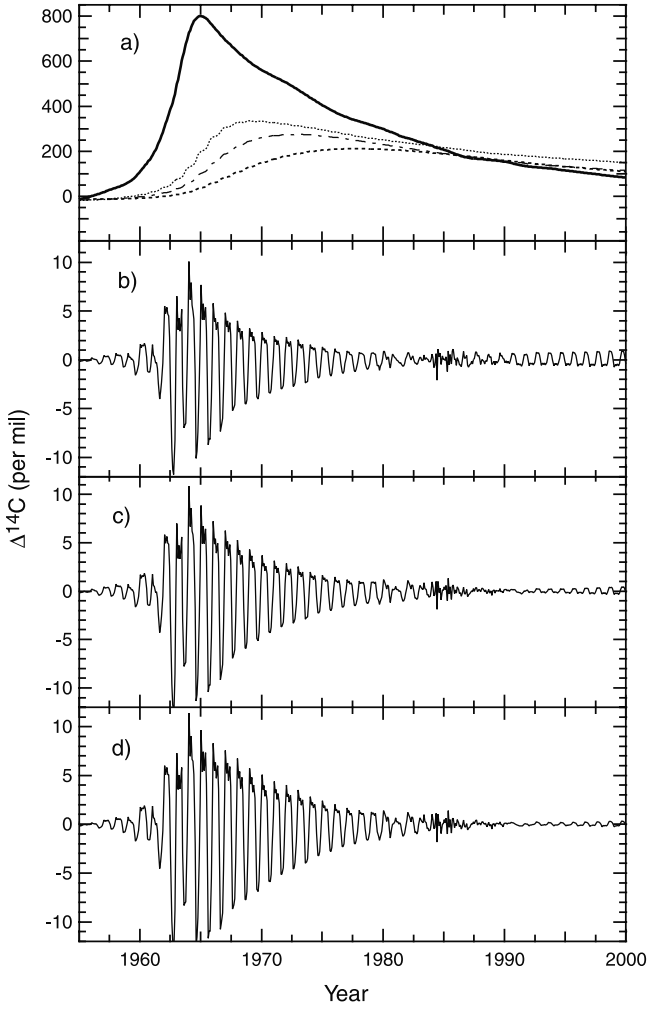

Figure 9. (a) The $\Delta^{14}C$ of heterotrophic respiration lags behind the atmosphere because of finite carbon residence times in plants, litter, and soils. In order of increasing mean residence time, heterotrophic respiration from biosphere scenarios 1–3 (Table 3) are given by the dotted, dashed-dotted, and dashed lines from regions north of 40°N. The solid thick line represents the overlying atmospheric $\Delta^{14}C$. (b–d) The biosphere contribution to the seasonal cycle of atmospheric $\Delta^{14}C$ at Fruholmen, Norway (71°N, 13°E), is shown for scenarios 1–3. In each scenario, the long-term trend was removed by application of a smoothing spline [*Enting*, 1987].

observed differences between Northern and Southern Hemisphere troposphere $\Delta^{14}C$ in the mid and late 1960s would have been considerably greater.

3.5. Combined Effects and Comparison With Observations

[48] At the time of the Test Ban treaty in 1963, stratospheric exchange was the dominant contributor to seasonal and latitudinal variation in troposphere $\Delta^{14}C$. With net extra-tropical stratosphere fluxes reaching a maximum during April and May in the Northern Hemisphere, we reproduced the phase and amplitude of the seasonal cycle of $\Delta^{14}C$ fairly well at Fruholmen in 1963, 1964, and 1965 (Figure 11a). By the late 1960s and early 1970s, however, model simulations considerably underestimated the amplitude of the observed seasonal cycle (Figure 12a). During this initial period, fluxes from the terrestrial biosphere contributed substantially to the $\Delta^{14}C$ seasonal cycle, with a phase that acted to cancel the stratospheric component (Figure 11a and Figure 12a).

[49] By the late 1980s, the stratospheric contribution had considerably weakened, but was still the dominant contributor to the seasonal cycle; the phase of the measured seasonal cycle at Fruholmen remained the same throughout the 30-year time series. Terrestrial biosphere (contributing ^{14}C-enriched summer respiration at this point) and fossil fuel fluxes were in phase with observed $\Delta^{14}C$ seasonal cycle, and amplified the stratospheric signal (Figure 11b). Again, the model simulations did fairly well at reproducing the phase of the seasonal cycle, but underestimated the amplitude in 1985, 1986, and 1987. During this latter period, fossil fuels were the second most important contributor, causing a decrease in $\Delta^{14}C$ during winter months, and in particular during February.

[50] At Wellington, New Zealand, the Northern Hemisphere stratospheric fluxes generated a seasonal cycle in the late 1960s and early 1970s that had about the same amplitude as the observations, but with a phase that lagged behind the observations by approximately 1.5 months. By the late 1980s, the northern stratospheric contribution had substantially weakened (Figures 6c and 6d).

[51] During the early 1970s, the latitudinal profile of $\Delta^{14}C$ was driven largely by stratosphere inputs in the Northern Hemisphere (Figure 13). By the late 1980s, the latitudinal profile had two minima (one at mid northern latitudes caused by fossil fuel emissions and a second at high-southern latitudes caused by exchange with the Southern Ocean) and three local maxima (South Pole, tropics, and North Pole). This latitudinal profile is qualitatively consistent with a north-south transect of atmospheric $\Delta^{14}C$ observations from the early 1990s [*Levin and Hesshaimer*, 2000]. In the tropics, both terrestrial ecosystems and tropical oceans created positive $\Delta^{14}C$ anomalies. In tropical forests, the $\Delta^{14}C$ of respiration in the late 1980s and 1990s was enriched because much of the carbon in vegetation and soils had residences times spanning several decades, and was

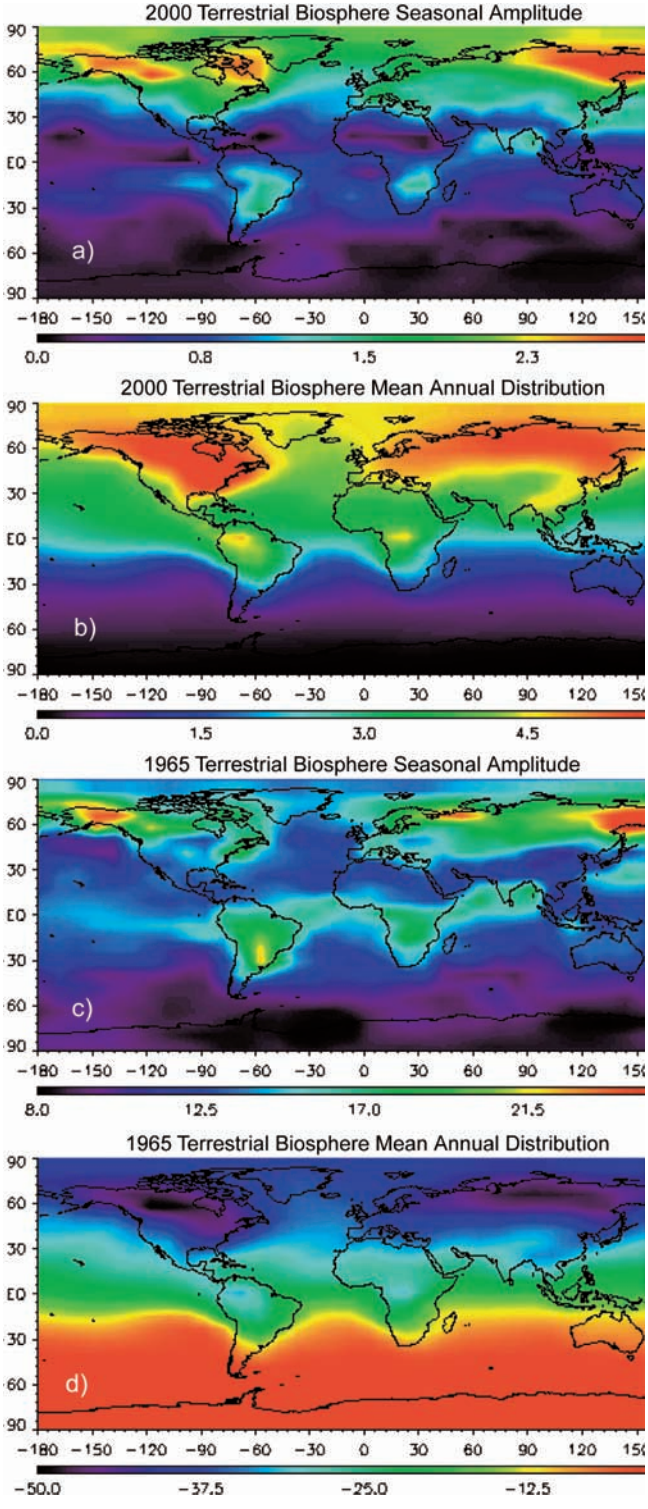

Figure 10. (opposite) The contribution of terrestrial biosphere fluxes in 2000 to (a) the seasonal amplitude of $\Delta^{14}C$ and (b) the mean annual $\Delta^{14}C$ (relative to the South Pole). The same two maps are presented for 1965 (c and d). Terrestrial biosphere fluxes are from scenario 1 (see text in section 2.6 and Table 3 for details). The mean annual $\Delta^{14}C$ values are relative to the South Pole. In 1965, fluxes from terrestrial ecosystems decreased Northern Hemisphere $\Delta^{14}C$ by 30‰ to 50‰, offsetting the injection of bomb ^{14}C from the Northern Hemisphere stratosphere that occurred at similar latitudes.

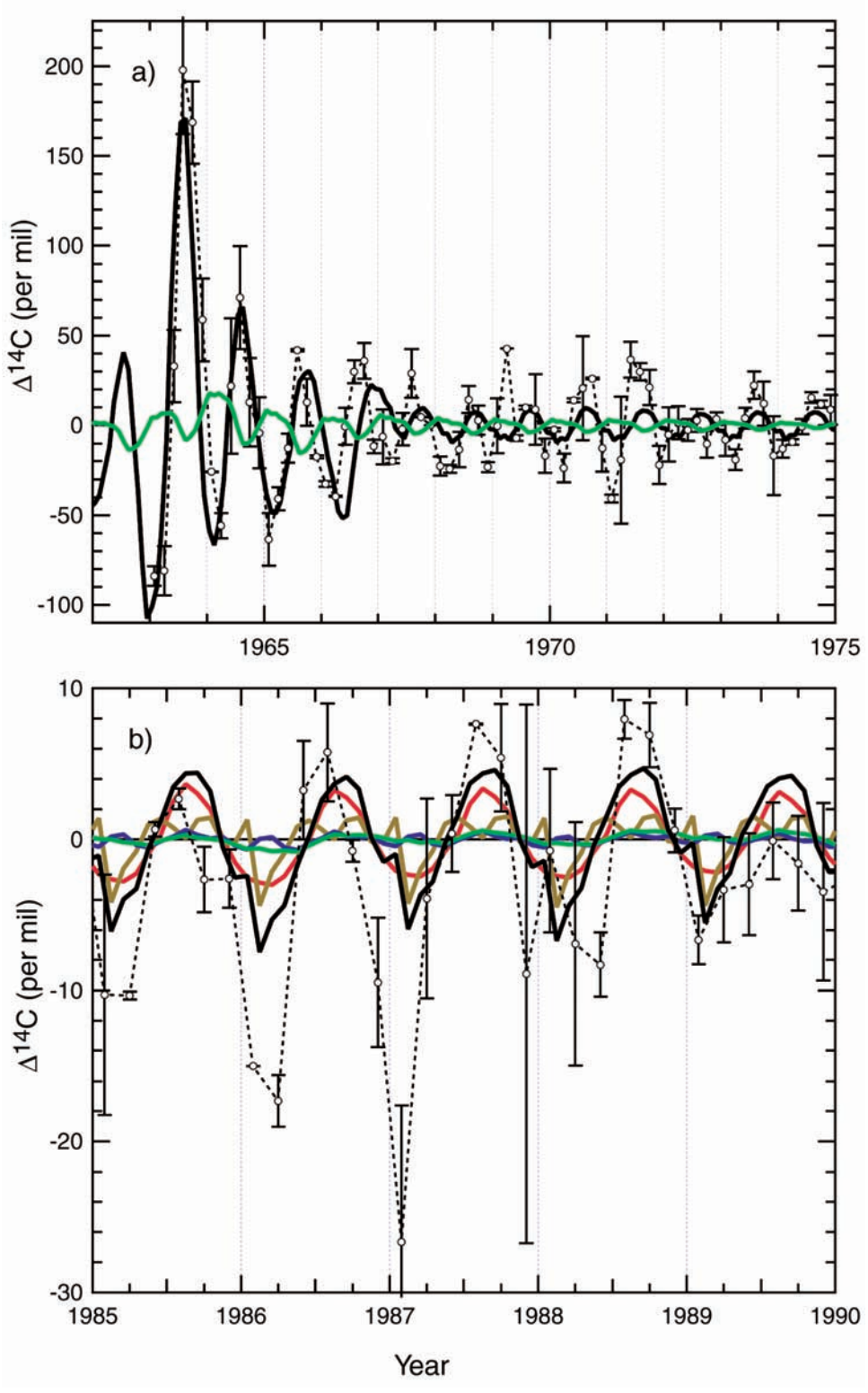

Figure 11. (a) Measurements from Fruholmen, Norway were detrended as described in the text and are shown with circles and standard deviation error bars [*Nydal and Lövseth*, 1996]. The solid black line represents the sum of fossil, ocean, stratosphere, and terrestrial biosphere model components from 1962 to 1975. The terrestrial biosphere component is separately represented by the green line. (b) Same as (a) but for the 1985 to 1990 period. The sum of fossil fuel (brown), ocean (blue), stratosphere (red), and terrestrial biosphere (green) components is represented by the solid black line.

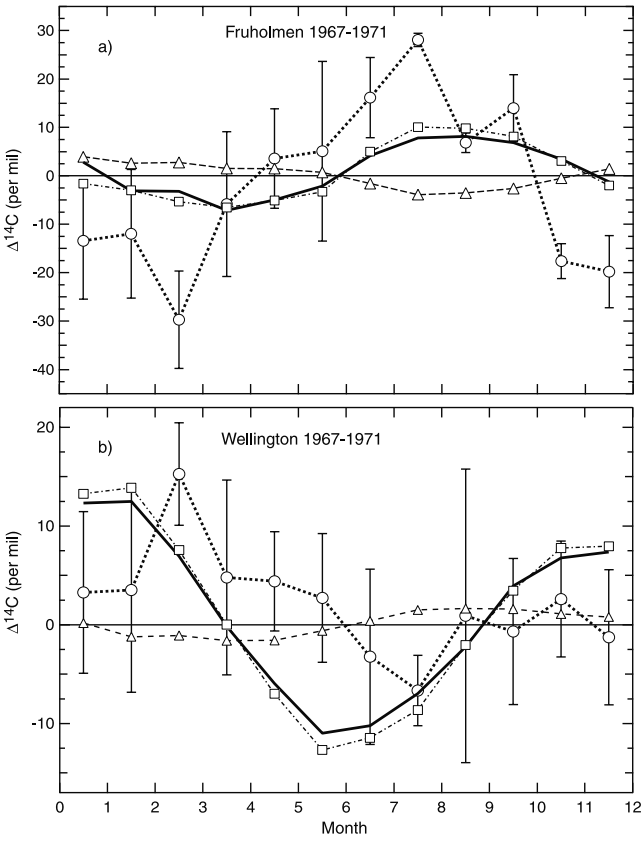

Figure 12. Modeled (solid line) and observed (dotted line and circles) seasonal cycles of $\Delta^{14}C$ for the 1967 to 1971 period at (a) Fruholmen, Norway, and (b) Wellington, New Zealand. At Fruholmen, the component of the seasonal cycle caused by respiration from the terrestrial biosphere (triangles and dashes) significantly offset the $\Delta^{14}C$ signal caused by fluxes from the stratosphere (squares and dashed-dotted line). Both observations and model long term trends were removed using cubic spline fit [*Enting*, 1987].

fixed when the atmosphere $\Delta^{14}C$ levels were much higher (Figure 10b). Likewise, in mid-ocean gyres, relatively shallow mixed layers and limited vertical entrainment of prebomb water masses has also led to mixed layer $\Delta^{14}C$ values that more closely tracked atmospheric $\Delta^{14}C$ levels as compared with high latitude oceans that were a stronger ^{14}C sink during this period.

3.6. The $\Delta^{14}C$ of Soil Respiration From Northern Ecosystems

[52] Measurements of $\Delta^{14}C$ in soil respiration from boreal forest and tundra ecosystems in Alaska in July of 2000 are summarized in Table 6. Summer respiration measurements from arctic tundra ecosystems near Toolik Lake, Alaska were near or below local atmospheric levels (~75‰), in contrast to boreal forest ecosystems in regions to the south (in interior Alaska) where soil respiration $\Delta^{14}C$ values were significantly higher (~112‰). One possible explanation for this difference in respired $\Delta^{14}C$ is that the more northern tundra ecosystems had slower rates of carbon cycling (as a result of colder temperatures and a shorter growing season),

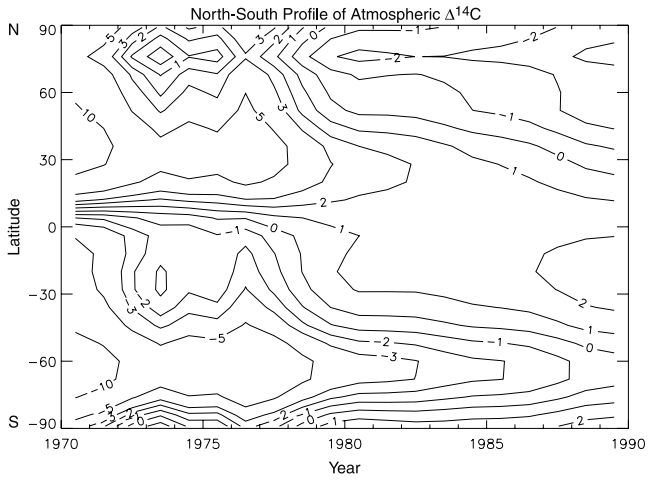

Figure 13. The latitudinal profile of mean annual $\Delta^{14}C$ from the sum of fossil fuel, ocean, stratosphere, and terrestrial biosphere fluxes is shown for the 1970 to 1990 period. By the late 1980s, the north-south profile had two local minima (northern mid latitudes and over the Southern Ocean) and three local maxima (North Pole, Southern Hemisphere tropics, and the South Pole. A 3-Megaton nuclear explosion detonated in 1975 significantly increased the north-south $\Delta^{14}C$ difference in 1976.

and thus had not yet undergone the crossover in respiration $\Delta^{14}C$ described in section 3.4 and shown in Figure 9a.

4. Discussion

4.1. Evolving Latitudinal Profile of $\Delta^{14}C$

[53] Over the last few decades, the processes that contribute to troposphere $\Delta^{14}C$ variability have dramatically shifted. The north-south profile significantly weakened from 1970 to 1990 (Figure 13), and surface measurements from the early 1990s suggest the north-south $\Delta^{14}C$ profile was nearly zero [*Levin and Hesshaimer*, 2000]. Based on our analysis of the component fluxes, we predict that the profile will continue to shift, with the Northern Hemisphere becoming progressively more ^{14}C-depleted as compared with the Southern Hemisphere over the next few decades. In addition, we predict a persistent local maximum in tropical $\Delta^{14}C$.

[54] As fossil fuel emissions continue to grow, it is likely that $\Delta^{14}C$ in the Northern Hemisphere will decrease from the direct infusion of fossil carbon with an isotopic signal of

Table 6. Latitudinal Profile of Observed $\Delta^{14}C$ in 2000 Summer Soil Respiration

Site	Latitude, °N	Number of Samples	Mean $\Delta^{14}C$, ‰	Standard Deviation,[a] ‰
Toolik Lake, AK	68	4	75	4
Caribou/Poker Creek, AK	65	4	106	12
Delta Junction, AK	64	8	119	10
Background Atmosphere	64 and 68	2	89	1

[a] The standard deviation reported here represents the variability across field samples. The precision of an individual AMS measurement is limited to ~± 5‰.

−1000‰. Gross CO_2 exchange with the Southern Ocean will counteract the impact of fossil fuel dilution in the north, with the strength of this offset depending both on the magnitude of the gross exchange and the residence times of dissolved inorganic carbon (DIC) in surface waters. Given that fossil fuel emissions are relatively well known, a limited atmospheric sampling program monitoring the shift in the north-south profile of atmospheric $\Delta^{14}C$ would have the potential to constrain the carbon dynamics of the Southern ocean [e.g., *Manning et al.*, 1990; *Levin and Hesshaimer*, 2000]. These observations could then be used to determine the latitudinal distribution of land and ocean carbon sinks via constraints on isotopic disequilibria for the $\delta^{13}C$ budget [e.g., *Ciais et al.*, 1995] or via constraints on regional ocean carbon fluxes when used in concert with observations of wind speed and ocean $\Delta^{14}C$ [*Wanninkhof*, 1992; *Key*, 1998].

[55] As compared with fossil fuel and ocean exchange, terrestrial ecosystems are likely to have a smaller, yet significant, impact on the north-south profile of $\Delta^{14}C$ over the next few decades. Differences between terrestrial ecosystems and the atmosphere currently enrich the Northern Hemisphere troposphere by about 5‰ and offset dilution by fossil fuels by about 25% (Figures 10b and 7b). The terrestrial contribution to the north-south gradient is likely to persist over the next several decades based on observations of decadal-scale turnover of carbon in northern extratropical ecosystems [*Trumbore*, 2000], but may weaken with more gradual declines in tropospheric $\Delta^{14}C$ [e.g, *Caldeira et al.*, 1998].

[56] Cosmogenic ^{14}C production, distributed approximately evenly within Northern and Southern hemisphere stratospheres, should have only a minor effect on the north-south profile as compared with fossil fuel emissions, and ocean and terrestrial biosphere isotopic disequilibria [*Braziunas et al.*, 1995]. In addition, while asymmetries in the strength of stratosphere-troposphere exchange in the Northern and Southern Hemisphere may have induced a north-south gradient in $\Delta^{14}C$ during the 1970s and 1980s (see section 3.3), our model analyses suggest that these effects were attenuated substantially by 2000, and will contribute far less than 1‰ variation to the north-south profile in the future.

[57] Over a period of several decades, basic features of the latitudinal profile visible in late 1980s in Figure 13 should remain intact (i.e., the 2 minima in northern mid latitudes and southern high latitudes, and the 3 maxima near the North Pole, equator, and South Pole). However, with continued fossil fuel burning over the next century, the oceans may ultimately become an atmospheric source of ^{14}C [*Caldeira et al.*, 1998], both regionally and globally. As this occurs, the contemporary minimum in $\Delta^{14}C$ observed in Southern Hemisphere high latitudes (Figure 13) eventually may be replaced by a maximum, because $\Delta^{14}C$ in these waters reflects exchange with intermediate waters that have a residence time of decades to centuries [*Toggweiler and Samuels*, 1993]. Specifically, the large mass of C involved with this circulation will equilibrate only very slowly with the atmosphere, and will impart a ocean to atmosphere flux with a $\Delta^{14}C$ level somewhere between preindustrial levels [*Braziunas et al.*, 1995], and the perturbation cause by the addition of bomb ^{14}C (Figure 1). If atmospheric $\Delta^{14}C$ drops below that of the ocean mixed layer in this region, then even the Southern Ocean will become a ^{14}C source. Other areas of the ocean with less intense vertical mixing (and shorter carbon residence times) such as the mid-ocean gyres and the tropics would be expected to more closely track decreasing atmospheric $\Delta^{14}C$ driven by fossil fuels.

4.2. Terrestrial Biosphere Process and Mechanism

[58] For terrestrial ecosystems, $\Delta^{14}C$ signals are imparted to the troposphere in proportion to the isotopic disequilibrium between NPP and heterotrophic respiration. Fractionation against ^{13}C and ^{14}C by photosynthesis, does not affect troposphere $\Delta^{14}C$ because $\Delta^{14}C$ is specifically defined to be insensitive to mass dependent fractionation [*Stuiver and Polach*, 1977]. While photosynthesis does not immediately affect tropospheric $\Delta^{14}C$, it does, of course, regulate the mass and $\Delta^{14}C$ content of carbon entering terrestrial ecosystems, and thus ultimately the magnitude of the respiration flux and the impact of the $\Delta^{14}C$ disequilibrium on the atmosphere in the future.

[59] The terrestrial biosphere contribution to the northern seasonal cycle of tropospheric $\Delta^{14}C$ arises because the $\Delta^{14}C$ composition of respiration and the atmosphere rapidly diverged in the 1960s (Figure 9a) and because in northern ecosystems heterotrophic respiration is primarily confined to summer and fall months, when microbial communities within the soil are warm and metabolically active [*Goulden et al.*, 1998]. In the 1960s, summer and fall heterotrophic respiration initially released a pulse of $\Delta^{14}C$-depleted CO_2 (relative to the local atmosphere), while more recently this pulse has become more $\Delta^{14}C$-enriched than the local atmosphere, because of lags associated with the decomposition of photosynthetic products fixed when atmospheric $\Delta^{14}C$ levels were high. During winter and early spring, when respiration rates are low, the atmosphere relaxes back to its initial state; atmospheric mixing removes the signal imparted at the surface by respiration during the summer.

[60] Our measurements of $\Delta^{14}C$ from black spruce forests in Alaska suggest that most terrestrial ecosystems now respire CO_2 that has a higher $\Delta^{14}C$ than the background atmosphere. We infer that most ecosystems are now a net ^{14}C source because rates of decomposition and carbon turnover are much higher in temperate and tropical ecosystems to the south, and so these ecosystems would more rapidly acquire the $\Delta^{14}C$ signal imparted by weapons testing (Figure 9a). Specifically, in high latitude ecosystems decomposition is limited by both temperature (a short growing season) and by chemically recalcitrant plant litter (e.g., needles and moss that have high lignin and low nitrogen content) [*Trumbore*, 1993; *Hobbie et al.*, 2000]. Within mature black spruce forests, allocation to wood further decreases rates of carbon turnover. Thus, our field observations suggest that the positive $\Delta^{14}C$ anomaly arising from northern terrestrial ecosystems in 2000 (Figure 10b) is basically correct (has the right sign); over 95% of heterotrophic respiration (and NPP) in the Northern Hemisphere extratropics (north of 20°N) originates from biomes other than Arctic tundra [*Randerson et al.*, 1997].

[61] In contrast, our measurements from the Arctic tundra suggest that even by the year 2000, some ecosystems in the far north still had respiration that was depleted in $\Delta^{14}C$ relative to the local atmosphere. This depletion was probably a result of slow carbon turnover rates and the decomposition of a significant amount of C fixed before the period of aboveground nuclear weapons testing. These conclusions are based on the assumption of more or less steady state conditions for ecosystem carbon cycling. Changes in ecosystem carbon cycling caused by local disturbance could also shift the $\Delta^{14}C$ of respired CO_2 to prebomb levels.

[62] The use of $\Delta^{14}C$ to quantify rapid turnover pools (less than 5 years) within ecosystems requires accurate measurements of local atmospheric $\Delta^{14}C$ [*Gaudinski et al.*, 2000; *Schuur et al.*, 2002]. Our analysis of spatial gradients in $\Delta^{14}C$ induced by fossil fuels, ocean, and terrestrial biosphere fluxes suggests that the $\Delta^{14}C$ of continental air may vary by 10‰ or more from season to season and from place to place. These results are consistent with observations from Europe that show large seasonal variability in the continental interior as compared with offshore ocean islands [*Levin et al.*, 1989; *Meijer et al.*, 1995]. For ecosystem studies exploring rapid turnover processes, our results confirm the idea that local atmospheric sampling made over the duration of the growing season, and weighted in proportion to rates of photosynthesis, are essential.

[63] Compared with any other place on Earth, it is possible that within the Amazon basin, the large one-way fluxes [*Grace et al.*, 1995; *Tian et al.*, 1998] and finite residence time of carbon within trees and soils [*de Camargo et al.*, 1999] may have significantly diluted near-surface atmospheric $\Delta^{14}C$ during the early 1960s. This temporary disequilibrium, lasting perhaps for a few months to a few years following the Test Ban Treaty, may have been recorded as a gradient in tree $\Delta^{14}C$ (with relatively enriched values near the coast and depleted values in the continental interior). The mechanism for such a gradient may be as follows. Within the northern and equatorial regions of the Amazon basin, air travels along the surface from the Atlantic towards the western continental interior and the Andes until it is removed from the system by convection [*Chou et al.*, in press]. At the coast, tree $\Delta^{14}C$ would have been high in 1963–1965, with marine boundary layer air being relatively enriched in $\Delta^{14}CO_2$. Interior tree $\Delta^{14}C$ may have been exposed to significantly lower values of $\Delta^{14}C$ because the CO_2 in air had undergone exchange (and partial replacement) by ecosystems that were upwind. Enhanced recycling of CO_2 within canopies in the Amazon interior would have enhanced the magnitude of this $\Delta^{14}C$ gradient [*Martinelli et al.*, 1991], even though it was not the primary mechanism.

[64] In our global analysis, we can see a trace of such a gradient (Figure 10d). However, several features of our coarse resolution modeling framework would cause us to underestimate its magnitude, including that we used only two tropical land basis regions and that the CO_2 taken up by terrestrial ecosystems in the Amazon was drawn from an average of the troposphere over much larger area of the tropics and subtropics, including deserts. Nevertheless, the high levels of NPP within the Amazon led to visible $\Delta^{14}C$ dilution in 1965 and enrichment in 2000 (Figures 10b and 10d). Trees from the interior Amazon have been measured and reflect $\Delta^{14}C$ values in the mid 1960s that are close to remote Southern Hemisphere observation stations [*Worbes and Junk*, 1989]. However, tree rings are difficult to measure in this region, and so a systematic study of coast to interior $\Delta^{14}C$ variability may be difficult; the mismatch of a single year (missing 1 growth increment) would significantly alter conclusions about the magnitude of the dilution.

4.3. Northern Hemisphere Seasonal Dynamics

[65] Even by the late 1980s, stratospheric fluxes were still the dominant contributor to the seasonal cycle at Fruholmen, Norway. Fluxes from the terrestrial biosphere initially attenuated the stratospheric signal, by ~10% from 1963 to 1966, and by ~25% from 1967 to 1971 (Figure 11a). By the late 1980s and early 1990s, the disequilibria of all the terrestrial scenarios had reversed sign, and were then in phase with the stratospheric tracer. Throughout the entire observational record at Fruholmen, we were able to reproduce the phase of the observations when northern stratospheric fluxes had a maximum in April and May, consistent with net flux estimates by *Appenzeller et al.* [1996] but in disagreement with other studies that have suggested tracer mixing with the troposphere is greatest in the Northern Hemisphere winter. While this result is probably sensitive to our tropospheric model, the GISS model behaves similarly to other tropospheric models in terms of the phase delay in transmitting a CO_2 tracer with a seasonal cycle from the surface to 200 mb [*Rayner and Law*, 1995]. Almost all of the models compared in the *Rayner and Law* [1995] study had a time delay of approximately 1 month for transmitting peak CO_2 levels in the spring from the surface to 200 mb, and between 1 and 2 months for the minimum in the fall.

[66] In contrast to our success in reproducing the phase of seasonal cycle, we substantially underestimated the amplitude at Fruholmen during several periods. Specifically, while we matched the amplitude from 1963 to 1966 and in 1988 and 1989, we underestimated the amplitude by at least a factor of 2 from 1967 to 1971 and from 1985 to 1988. There are several possible reasons for this, and probably more than one process is at work.

[67] First, the version of GISS atmospheric tracer model that had only nine vertical levels did not explicitly resolve planetary boundary layer (PBL) dynamics. Because the PBL traps surface fluxes at night and during winter [*Denning et al.*, 1996], our model simulations may have underestimated the contribution of fossil fuel emissions and other surface sources during winter (and may have simultaneously overestimated contributions from the stratosphere). Along similar lines, Fruholmen is relatively close to the industrial center of Europe. If we underestimated the seasonality of the fossil fuel source, or its transport to the grid cell in our model containing the coordinates for Fruholmen, it would have had a large impact on the seasonal cycle of $\Delta^{14}C$ because of its extreme isotopic composition (−1000‰), but only a minor impact on the seasonal cycle of CO_2 (Figure 4) [*Randerson et al.*, 1997].

[68] Second, NaOH solution traps that were used extensively to measure tropospheric $\Delta^{14}C$ at the surface sampled

the atmosphere in a way that is different from what might be expected from flask sampling in the middle of the day or from a monthly mean extracted from an atmospheric model [*Hesshaimer and Levin*, 2000]. Averaging day and night (typically for a period of a week or two) NaOH traps would have integrated over both turbulent and stable atmospheric periods. However, since the total CO_2 taken up by the NaOH trap is partly controlled by diffusion, periods with higher levels of atmospheric CO_2 in the boundary layer (i.e., night) may have contributed to more of the total dissolved inorganic carbon in solution than well-mixed periods (i.e., day). This effect may have amplified the contribution of fossil fuel emissions during winter months. We did not try to estimate or account for this potential model-data mismatch by resampling our atmospheric model: monthly mean concentrations from the atmospheric model were directly compared with observations derived from NaOH traps.

[69] Third, cosmogenic ^{14}C production is affected by solar cycles on decadal and centennial timescales [*Bard et al.*, 1997]. In addition, the magnitude of stratospheric mixing with the troposphere is quite variable from year to year [*Gettelman and Sobel*, 2000]. Our stratosphere and troposphere models did not attempt to account for these interannually varying processes.

[70] Finally, our terrestrial biosphere model was simplified so that all the carbon pools in the model (plants, litter, and soils) were driven with a single monthly value of air temperature. Thus, the relative contribution of different pools to the respiration flux did not change much from month-to-month (there was a small change from the increase in total biomass during the growing season in rapidly exchanging pools). The impact of terrestrial ecosystems on the seasonal dynamics of atmospheric $\Delta^{14}C$ in our model was caused largely by the magnitude of respiration being much greater in summer than in winter. In contrast to our model structure, observations from the boreal forest show that as plants and surface soils freeze during fall and winter, the $\Delta^{14}C$ of soil respiration drops below atmospheric levels [*Winston et al.*, 1997]. This drop reflects the very slow turnover of soils at depth that are not yet frozen and still metabolically active. However, this mechanism should contribute only minimally to atmospheric forcing due to the relatively low CO_2 flux rates during this time.

4.4. Southern Hemisphere Seasonal Dynamics

[71] As mentioned in section 1, the seasonal amplitude of $\Delta^{14}C$ from Wellington, New Zealand decreased from 1967 to 1980 from about 20‰ to 3‰ [*Manning et al.*, 1990]. Model simulations by *Manning et al.* [1990] in which bomb ^{14}C was distributed evenly across the stratosphere in both the Northern and Southern Hemispheres generated a seasonal cycle at Wellington that was almost completely out of phase with the observations. Here, we were able to reproduce the amplitude and most of the phase of the Wellington $\Delta^{14}C$ seasonal cycle in the late 1960s and early 1970s by distributing ^{14}C in the Northern and Southern Hemisphere stratosphere according to the latitude of the detonations, and by assuming that no north-south mixing occurred across the equator in the stratosphere. The importance of Northern hemisphere extratropical stratosphere flux (in term of explaining the seasonal signal at Wellington) is consistent with hemispheric asymmetries in weapons detonation (Table 1), the large seasonal amplitudes observed at mid and high northern latitudes [*Telegadas*, 1971], and the time delays and attenuation associated with the transmission of seasonal signals across the equator observed for other tracers (i.e., CO_2).

[72] From 1980 to 1987, a second seasonal cycle with a smaller amplitude emerged at Wellington, with a peak in July and August and a minimum in January and an amplitude of ~6‰ [*Manning et al.*, 1990]. The emergence of a second seasonal cycle is consistent with the decline of the Northern Hemisphere stratosphere component in the mid 1970s and the emergence of underlying seasonal contribution from the Southern Hemisphere stratosphere or Southern Hemisphere oceans (Figure 6). We were unable to resolve this transition with our model. This may have been a limitation of aggregating our ocean fluxes (we averaged over the entire South Pacific from 0°S to 48°S for the pulse model) or misrepresentation of the Southern Hemisphere stratospheric flux.

5. Conclusions

[73] While atmospheric CO_2 and $\delta^{13}C$ distributions are sensitive to net CO_2 fluxes, atmospheric $\Delta^{14}C$ is a unique tracer because its atmospheric distribution depends mostly on gross exchange with ocean and terrestrial biosphere reservoirs, fossil fuel use, and stratospheric inputs. Net carbon sinks have almost no impact on tropospheric $\Delta^{14}C$, making this tracer ideal for constraining the residence times of carbon reservoirs interacting with the atmosphere. The distribution of tropospheric $\Delta^{14}C$ near the surface depends largely on three factors: 1) the magnitude of gross CO_2 fluxes from the stratosphere and surface, 2) the $\Delta^{14}C$ content of these gross fluxes (e.g., the age of the respired carbon from terrestrial ecosystems), and 3) the time a packet of air remains in contact with the surface (i.e., the strength of planetary boundary layer mixing). While preliminary, we draw the following conclusions from our analysis.

[74] First, the full 30-year time series of $\Delta^{14}C$ observations from the surface at Fruholmen, Norway provides an important and underutilized constraint on the seasonality of extra-tropical stratospheric fluxes in the Northern Hemisphere. Net stratospheric fluxes that peak in late spring (April and May) in the Northern hemisphere extra tropics are most consistent with the observed distribution of the $\Delta^{14}C$ tracer in the troposphere. Using the spatially resolved ^{14}C flux estimates from the terrestrial biosphere developed here, along with recently revised $\Delta^{14}C$ measurements from the free troposphere and stratosphere [*Hesshaimer and Levin*, 2000], it now feasible to formally invert for the monthly distribution of the stratospheric flux.

[75] Second, heterotrophic respiration from terrestrial ecosystems (that was initially ^{14}C depleted) partially cancelled seasonal oscillations of $\Delta^{14}C$ caused by stratospheric fluxes during the mid and late 1960s. Similarly, terrestrial biosphere fluxes significantly counteracted the large north-south difference in $\Delta^{14}C$ caused by the injection of ^{14}C from Northern Hemisphere stratosphere-troposphere exchange during this period.

[76] Third, the $\Delta^{14}C$ content of fluxes in many terrestrial ecosystems and in some ocean regions has (or will) reverse seasonal phase as bomb ^{14}C cycles through internal reservoirs with decadal timescales.

[77] Fourth, it is possible to account for much of the amplitude and phase of the $\Delta^{14}C$ seasonal cycle at Wellington, New Zealand during the 1960s and 1970s by distributing most of the bomb radiocarbon in the Northern hemisphere stratosphere.

[78] Fifth, the latitudinal profile of $\Delta^{14}C$ will continue to shift over the next few decades, with the Southern Hemisphere troposphere becoming progressively more ^{14}C-enriched as compared with the Northern Hemisphere. Measuring the profile would provide strong constraints on the latitudinal distribution of combined ocean and land carbon residence times, and thus ultimately the potential of these reservoirs to serve as carbon sinks.

[79] **Acknowledgments.** We wish to thank J. Adkins, C. Masiello, and K. Treseder for discussion and for comments on previous versions of this manuscript, two anonymous reviewers for constructive suggestions, and J. John for technical assistance with the GISS tracer model. This work was supported by a NASA IDS grant NAG5-9462. We are also grateful to I. Levin, K. Lövseth, M. Manning, R Nydal, and others for the very long time series of atmospheric $\Delta^{14}C$ that have been made publicly available at the Carbon Dioxide Information Analysis Center.

References

Andres, R. J., G. Marland, I. Y. Fung, and E. Matthews, A $1° \times 1°$ distribution of carbon dioxide emissions from fossil fuel consumption and cement manufacture, 1950–1990, *Global Biogeochem. Cycles*, *10*(3), 419–430, 1996.

Andrews, A. E., et al., Mean ages of stratospheric air derived from in situ observations of CO_2, CH_4, and N_2O, *J. Geophys. Res.*, *106*(D23), 32,295–32,314, 2001.

Appenzeller, C., J. R. Holton, and K. H. Rosenlof, Seasonal variation of mass transport across the tropopause, *J. Geophys. Res.*, *101*(D10), 15,071–15,078, 1996.

Balesdent, J., The turnover of soil organic fractions estimated by radiocarbon dating, *Sci. Total Environ.*, *62*, 405–408, 1987.

Bard, E., G. M. Raisbeck, F. Yiou, and J. Jouzel, Solar modulation of cosmogenic nuclide production over the last millenium: Comparison between ^{14}C and ^{10}Be records, *Earth Planet. Sci. Lett.*, *150*, 453–462, 1997.

Bauer, J., P. M. Williams, and E. R. M. Druffel, Recovery of sub-milligram quantities of carbon dioxide from gas streams by molecular sieve for subsequent determination of isotopic natural abundance, *Anal. Chem.*, *64*, 824–827, 1992.

Bishop, J. K. B., and W. B. Rossow, Spatial and temporal variability of global surface solar irradiance, *J. Geophys. Res.*, *96*, 16,839–16,858, 1991.

Boering, K. A., S. C. Wofsy, B. C. Daube, H. R. Schneider, M. Loewenstein, and J. R. Podolske, Stratospheric mean ages and transport rates from observations of carbon dioxide and nitrous oxide, *Science*, *274*(5291), 1340–1343, 1996.

Braziunas, T. F., I. Y. Fung, and M. Stuiver, The preindustrial atmospheric $^{14}CO_2$ latitudinal gradient as related to exchanges among atmospheric, oceanic, and terrestrial reservoirs, *Global Biogeochem. Cycles*, *9*(4), 565–584, 1995.

Broecker, W. S., and T. H. Peng, Stratospheric contribution to the global bomb radiocarbon inventory - model versus observation, *Global Biogeochem. Cycles*, *8*(3), 377–384, 1994.

Broecker, W. S., S. Sutherland, W. Smethie, T. H. Peng, and G. Ostlund, Oceanic radiocarbon—separation of the natural and bomb components, *Global Biogeochem. Cycles*, *9*(2), 263–288, 1995.

Caldeira, K., G. H. Rau, and P. B. Duffy, Predicted net efflux of radiocarbon from the ocean and increase in atmospheric radiocarbon content, *Geophys. Res. Lett.*, *25*(20), 3811–3814, 1998.

Chou, W. W., S. C. Wofsy, R. C. Harriss, J. C. Lin, C. Gerbig, and G. W. Sachse, Net fluxes of CO_2 in Amazonia derived from aircraft observations, *J. Geophys. Res.*, *107*, doi:10.1029/2001JD001295, in press, 2002.

Ciais, P., P. P. Tans, J. W. C. White, M. Trolier, R. J. Francey, J. A. Berry, D. A. Randall, P. J. Seller, J. G. Collatz, and D. S. Schimel, Partitioning ocean and land uptake of CO_2 as inferred by $\delta^{13}C$ measurements from the NOAA Climate Monitoring and Diagnostics Laboratory global air sampling network, *J. Geophys. Res.*, *100*(D3), 5051–5070, 1995.

de Camargo, P. B., S. E. Trumbore, L. A. Martinelli, E. A. Davidson, D. C. Nepstad, and R. L. Victoria, Soil carbon dynamics in regrowing forest of eastern Amazonia, *Global Change Biol.*, *5*(6), 693–702, 1999.

Denning, S. A., D. A. Randall, G. J. Collatz, and P. J. Sellers, Simulations of terrestrial carbon metabolism and atmospheric CO_2 in a general-circulation model, 2, Simulated CO_2 concentrations, *Tellus, Ser. B*, *48*, 543–567, 1996.

Duffy, P. B., and K. Caldeira, 3-dimensional model calculation of ocean uptake of bomb C-14 and implications for the global budget of bomb C-14, *Global Biogeochem. Cycles*, *9*(3), 373–375, 1995.

Duffy, P. B., K. Caldeira, J. Selvaggi, and M. I. Hoffert, Effects of subgrid-scale mixing parameterizations on simulated distributions of natural C-14, temperature, and salinity in a three-dimensional ocean general circulation model, *J. Phys. Oceanogr.*, *27*(4), 498–523, 1997.

Enting, I. G., *Nuclear Weapons Data for Use in Carbon Cycle Modeling*, pp. 1–18, Commonwe. Sci. and Ind. Res. Organ., Melbourne, Australia, 1982.

Enting, I. G., On the use of smoothing splines to filter CO_2 data, *J. Geophys. Res.*, *92*(D9), 10,977–10,984, 1987.

Enting, I. G., and J. V. Mansbridge, Preliminary studies with a two-dimensional model using transport fields derived from a GCM, in *CSIRO-ABM Meeting on The Scientific Applications of Baseline Observations of Atmospheric Constituents, Tech. Pap. 14*, pp. 1–47, Commonw. Sci. and Ind. Res. Organ., Melbourne, Australia, 1987.

Fung, I. Y., J. John, J. Lerner, E. Matthews, M. Prather, L. P. Steele, and P. J. Fraser, Three dimensional model synthesis of the global methane cycle, *J. Geophys. Res.*, *96*(D7), 13,033–13,065, 1991.

Gaudinski, J. B., S. E. Trumbore, E. A. Davidson, and S. H. Zheng, Soil carbon cycling in a temperate forest: Radiocarbon-based estimates of residence times, sequestration rates and partitioning of fluxes, *Biogeochemistry*, *51*(1), 33–69, 2000.

Gettelman, A., and A. H. Sobel, Direct diagnoses of stratosphere-troposphere exchange, *J. Atmos. Sci.*, *57*(1), 3–16, 2000.

Glasstone, S., and P. J. Dolan, *The Effects of Nuclear Weapons*, 3rd ed., 653 pp., U.S. Dep. of Def. and U.S. Dep. of Energy, Washington, D. C., 1977.

Goulden, M. L., et al., Sensitivity of boreal forest carbon balance to warming, *Science*, *279*, 214–217, 1998.

Grace, J., et al., Carbon dioxide uptake by an undisturbed tropical rain forest in southwest Amazonia, *Science*, *270*, 778–780, 1995.

Guilderson, T. P., and D. P. Schrag, Abrupt shift in subsurface temperatures in the Tropical Pacific associated with changes in El Nino, *Science*, *281*(5374), 240–243, 1998.

Gurney, K. R., et al., Toward robust regional estimates of CO_2 sources and sinks using atmospheric transport models, *Nature*, *415*(6872), 626–630, 2002.

Harrison, K. G., W. S. Broecker, and G. Bonani, The effect of changing land use on soil radiocarbon, *Science*, *262*, 725–726, 1993.

Hesshaimer, V., and I. Levin, Revision of stratospheric bomb $^{14}CO_2$ inventory, *J. Geophys. Res.*, *105*(D9), 11,641–11,658, 2000.

Hesshaimer, V., M. Heimann, and I. Levin, Radiocarbon evidence for a smaller oceanic carbon dioxide sink than previously believed, *Nature*, *370*, 201–203, 1994.

Hobbie, S., J. P. Schimel, S. E. Trumbore, and J. T. Randerson, Controls over carbon storage and turnover in high-latitude soils, *Global Change Biol.*, *6*, 196–210, 2000.

Holton, J. R., P. H. Haynes, M. E. McIntyre, A. R. Douglass, R. B. Rood, and L. Pfister, Stratosphere-troposhere exchange, *Rev. Geophys.*, *33*(4), 403–439, 1995.

Jain, A. K., H. S. Kheshgi, and D. J. Wuebbles, A globally aggregated reconstruction of cycles of carbon and its isotopes, *Tellus, Ser. B*, *48*, 583–600, 1996.

Johnston, H. S., D. Kattenhorn, and G. Whitten, Use of excess carbon 14 data to calibrate models of stratospheric ozone depletion by supersonic transports, *J. Geophys. Res.*, *81*(3), 368–380, 1976.

Keeling, C. D., R. B. Bacastow, A. F. Carter, S. C. Piper, T. P. Whorf, M. Heimann, W. G. Mook, and H. Roeloffzen, A three-dimensional model of atmospheric CO_2 transport based on observed winds, 1, Analysis of observational data, in *Aspects of Climate Variability in the Pacific and the Western Americas*, *Geophys. Monogr. Ser.*, vol. 55, edited by D. H. Peterson, pp. 165–236, AGU, Washington, D. C., 1989.

Key, R. M., Early results from the WOCE radiocarbon program, in *TYKKI Workshop Report*, Jpn. Sci. and Technol. Agency, Tokyo, Japan, 1998.

Lassey, K. R., I. G. Enting, and C. M. Trudinger, The earth's radiocarbon budget, a constant model of the global carbon and radiocarbon cycles, *Tellus, Ser. B*, *48*(4), 487–501, 1996.

Levin, I., and V. Hesshaimer, Radiocarbon—a unique tracer of global carbon cycle dynamics, *Radiocarbon*, *42*(1), 69–80, 2000.

Levin, I., K. O. Munnich, and W. Weiss, The effect of anthropogenic CO_2 and ^{14}C sources on the distribution of ^{14}C in the atmosphere, *Radiocarbon*, *22*(2), 379–391, 1980.

Levin, I., J. Schuchard, B. Kromer, and K. O. Munnich, The continental European Suess-Effect, *Radiocarbon*, *31*, 431–440, 1989.

Levin, I., R. Graul, and N. B. A. Trivett, Long-term observations of atmospheric CO_2 and carbon isotopes at continental sites in Germany, *Tellus, Ser. B*, *47*, 23–34, 1995.

Lingenfelter, R. E., Production of carbon 14 by cosmic ray neutrons, *Rev. Geophys.*, *1*, 35–55, 1963.

Los, S. O., C. O. Justice, and C. J. Tucker, A global 1 × 1 NDVI data set for climate studies derived from GIMMS continental NDVI data, *Int. J. Remote Sens.*, *15*(17), 3493–3518, 1994.

Mahlman, J. D., and W. J. Moxim, Tracer simulation using a global general circulation model: Results from a midlatitude instantaneous source experiment, *J. Atmos. Sci.*, *35*, 1340–1374, 1978.

Manning, M. R., D. C. Lowe, W. H. Melhuish, R. J. Sparks, G. Wallace, C. A. M. Brenninkmeijer, and R. C. McGill, The use of radiocarbon measurements in atmospheric studies, *Radiocarbon*, *32*(1), 37–58, 1990.

Marland, G., T. Boden, and R. J. Andres, *Global, Regional, and National Annual CO_2 Emissions From Fossil-Fuel Burning, Hydraulic Cement Production, and Gas Flaring: 1751–1997*, Carbon Dioxide Inf. and Anal. Cent., Oak Ridge, Tenn., 2000.

Martinelli, L. A., A. H. Devol, R. L. Victoria, and J. E. Richey, Stable carbon isotope variation in C3 and C4 plants along the Amazon River, *Nature*, *353*(6339), 57–59, 1991.

McGuire, A. D., et al., Carbon balance of the terrestrial biosphere in the twentieth century: Analyses of CO_2, climate and land use effects with four process-based ecosystem models, *Global Biogeochem. Cycles*, *15*(1), 183–206, 2001.

Meijer, H. A. J., J. van der Plicht, J. S. Gislefoss, and R. Nydal, Comparing long-term atmospheric ^{14}C and ^{3}H records near Groningen, Netherlands with Fruholmen, Norway and Izana, Canary Islands ^{14}C Stations, *Radiocarbon*, *37*(1), 39–50, 1995.

Nydal, R., and K. Lövseth, Tracing bomb ^{14}C in the atmosphere 1962–1980, *J. Geophys. Res.*, *88*(C6), 3621–3642, 1983.

Nydal, R., and K. Lövseth, *Carbon-14 Measurements in Atmospheric CO_2 From Northern and Southern Hemisphere Sites, 1962–1993*, 67 pp., Carbon Dioxide Inf. Anal. Cent., Oak Ridge Natl. Lab., Oak Ridge, Tenn., 1996.

Oeschger, H., U. Siegenthaler, U. Schotterer, and A. Gugelmann, A box diffusion model to study the carbon dioxide exchange in nature, *Tellus XXVII*, *2*, 168–192, 1975.

Orr, J. C., et al., Estimates of anthropogenic carbon uptake from four three-dimensional global ocean models, *Global Biogeochem. Cycles*, *15*(1), 43–60, 2001.

Randerson, J. T., M. V. Thompson, T. J. Conway, I. Y. Fung, and C. B. Field, The contribution of terrestrial sources and sinks to trends in the seasonal cycle of atmospheric carbon dioxide, *Global Biogeochem. Cycles*, *11*, 535–560, 1997.

Randerson, J. T., et al., Carbon isotope discrimination of arctic and boreal biomes inferred from remote atmospheric measurements and a biosphere-atmosphere model, *Global Biogeochem. Cycles*, *16*(3), 1028, doi:10.1029/2001GB001435, 2002.

Rasch, P. J., X. Tie, B. A. Boville, and D. L. Williamson, A three-dimensional transport model for the middle atmosphere, *J. Geophys. Res.*, *99*(D1), 999–1017, 1994.

Rayner, P., R. M. Law, A comparison of modelled responses to prescribed CO_2 sources, *Tech. Pap. 36*, pp. 1–82, CSIRO Div. Atmos. Res., Melbourne, 1995.

Rodgers, K. B., D. P. Schrag, M. A. Cane, and N. H. Naik, The bomb C-14 transient in the Pacific Ocean, *J. Geophys. Res.*, *105*(C4), 8489–8512, 2000.

Rotty, R. M., Estimates of seasonal variation in fossil fuel CO_2 emissions, *Tellus, Ser. B*, *39*, 184–202, 1987.

Rozanski, K., I. Levin, J. Stock, R. E. G. Falcon, and F. Rubio, Atmospheric (CO_2)-C-14 variations in the Equatorial region, *Radiocarbon*, *37*(2), 509–515, 1995.

Running, S., D. Baldocchi, D. Turner, S. Gower, P. Bakwin, and K. Hibbard, A global terrestrial monitoring network integrating tower fluxes, flask sampling, ecosystem modeling, and EOS satellite data, *Remote Sens. Environ.*, *70*, 108–127, 1999.

Schuur, E. A. G., M. C. Mack, J. W. Harden, and S. E. Trumbore, The isotopic composition of carbon dioxide from a boreal forest fire: Inferring carbon loss from measurements and modeling, *Global Biogeochem. Cycles*, *16*, 10.1029/2001GB001840, in press, 2002.

Shia, R.-L., Y. L. Yung, M. Allen, R. W. Zurek, and D. Crisp, Sensitivity study of advection and diffusion coefficients in a two-dimensional stratospheric model using excess carbon 14 data, *J. Geophys. Res.*, *94*(D15), 18,467–18,484, 1989.

Siegenthaler, U., Uptake of Excess CO_2 by an outcrop-diffusion model of the ocean, *J. Geophys. Res.*, *88*(C6), 3599–3608, 1983.

Siegenthaler, U., and F. Joos, Use of a simple model for studying oceanic tracer distributions and the global carbon cycle, *Tellus, Ser. B*, *44*, 186–207, 1992.

Stuiver, M., and H. A. Polach, Discussion: Reporting of ^{14}C data, *Radiocarbon*, *19*, 355–363, 1977.

Stuiver, M., P. J. Reimer, and T. F. Braziunas, High-precision radiocarbon age calibration for terrestrial and marine samples, *Radiocarbon*, *40*, 1127–1151, 1998.

Tans, P., A compilation of bomb ^{14}C data for use in global carbon model calculations, in *Carbon Cycle Modeling*, edited by B. Bolin, pp. 131–157, John Wiley, New York, 1981.

Tans, P. P., I. Y. Fung, and T. Takahashi, Observation constraints on the global atmospheric CO_2 budget, *Science*, *247*, 1431–1438, 1990.

Telegadas, K., The seasonal atmospheric distribution and inventories of excess carbon-14 from March 1955 to July 1969, *HASL-243*, pp. 2–86, Health and Safety Lab., U.S. At. Energy Comm., New York, 1971.

Thompson, M. V., and J. T. Randerson, Impulse response functions of terrestrial carbon cycle models: Method and application, *Global Change Biol.*, *5*, 371–394, 1999.

Thompson, M. V., J. T. Randerson, C. M. Malmstrom, and C. B. Field, Change in net primary production and heterotrophic respiration: How much is necessary to sustain the terrestrial carbon sink?, *Global Biogeochem. Cycles*, *10*, 711–726, 1996.

Tian, H. Q., J. M. Melillo, D. W. Kicklighter, A. D. McGuire, J. V. K. Helfrich, B. Moore, and C. J. Vorosmarty, Effect of interannual climate variability on carbon storage in Amazonian ecosystems, *Nature*, *396*(6712), 664–667, 1998.

Toggweiler, J. R., and B. Samuels, New radiocarbon constraints on the upwelling of abyssal water, in *The Global Carbon Cycle*, edited by M. Heimann, pp. 333–366, Springer-Verlag, New York, 1993.

Trolier, M., J. W. C. White, P. P. Tans, K. A. Masarie, and P. A. Gemery, Monitoring the isotope composition of atmospheric CO_2: Measurements from the NOAA Global Air Sampling Network, *J. Geophys. Res.*, *101*(D20), 25,897–25,916, 1996.

Trumbore, S. E., Comparison of carbon dynamics in tropical and temperate soils using radiocarbon measurements, *Global Biogeochem. Cycles*, *7*(2), 275–290, 1993.

Trumbore, S. E., Age of soil organic matter and soil respiration: Radiocarbon constraints on belowground C dynamics, *Ecol. Appl.*, *10*(2), 399–411, 2000.

Trumbore, S. E., O. A. Chadwick, and R. Amundson, Rapid exchange between soil carbon and atmospheric carbon dioxide driven by temperature change, *Science*, *272*, 393–396, 1996.

Vogel, J. S., A rapid method for preparation of biomedical targets for AMS, *Radiocarbon*, *34*, 344–350, 1992.

Wanninkhof, R., Relationship between wind speed and gas-exchange over the ocean, *J. Geophys. Res.*, *97*(C5), 7373–7382, 1992.

Winston, G. C., E. T. Sundquist, B. B. Stephens, and S. E. Trumbore, Winter CO_2 fluxes in a boreal forest, *J. Geophys. Res.*, *102*(D24), 28,795–28,804, 1997.

Worbes, M., and J. Junk, Dating tropical trees by means of ^{14}C from bomb tests, *Ecology*, *70*, 503–507, 1989.

K. Caldeira, Climate System Modeling Group, Lawrence Livermore National Laboratory, University of California, 7000 East Avenue, L-256, Livermore, CA 94550, USA. (kenc@llnl.gov)

I. G. Enting, CSIRO Atmospheric Research, PMB 1, Aspendale, Victoria 3195, Australia. (ian.enting@dar.csiro.au)

I. Y. Fung, Center for Atmospheric Sciences, University of California Berkeley, McCone Hall 4767, Berkeley, CA 94720-4767, USA. (inez@atmos.berkeley.edu)

J. T. Randerson, Divisions of Geological and Planetary Sciences and Engineering and Applied Science, California Institute of Technology, Mail Stop 100-23, Pasadena, CA 91125, USA. (jimr@gps.caltech.edu)

E. A. G. Schuur, Department of Botany, University of Florida, PO Box 118526, Gainesville, FL 32611-8526, USA. (tschuur@ufl.edu)